

PARAMETER ESTIMATION TECHNIQUES FOR DETERMINING SAFE VEHICLE  
SPEEDS IN UGVs

Except where reference is made to the work of others, the work described in this thesis is my own or was done in collaboration with my advisory committee. This thesis does not include proprietary or classified information.

---

Dustin L. Edwards

Certificate of Approval:

---

George T. Flowers  
Alumni Professor  
Mechanical Engineering

---

David M. Bevly, Chair  
Associate Professor  
Mechanical Engineering

---

David Beale  
Professor  
Mechanical Engineering

---

Joe F. Pittman  
Interim Dean  
Graduate School

PARAMETER ESTIMATION TECHNIQUES FOR DETERMINING SAFE VEHICLE  
SPEEDS IN UGVs

Dustin L. Edwards

A Thesis  
Submitted to  
the Graduate Faculty of  
Auburn University  
in Partial Fulfillment of the  
Requirements for the  
Degree of  
Master of Science

Auburn, Alabama  
May 10, 2008

PARAMETER ESTIMATION TECHNIQUES FOR DETERMINING SAFE VEHICLE  
SPEEDS IN UGVs

Dustin L. Edwards

Permission is granted to Auburn University to make copies of this thesis at its discretion, upon the request of individuals or institutions and at their expense. The author reserves all publication rights.

---

Signature of Author

---

Date of Graduation

## VITA

Dustin was born February 9, 1982, the third child of James and Kathy Edwards. Born and raised in Pisgah, Alabama, he attended Rosalie Elementary School and Pisgah High School, after which, he decided to begin his college career at Northeast Alabama Community College and later Auburn University, resulting in many wonderful friends, fond memories, and a Bachelor of Science degree in Mechanical Engineering. As an undergraduate, Dustin graduated Summa Cum Laude as one of the top students in his class. After his undergraduate studies were completed, he continued his education by staying at Auburn University and working on his Masters of Science degree in Mechanical Engineering, under Dr. David Bevly in the GPS and Vehicle Dynamics Lab (Gavlab).

THESIS ABSTRACT  
PARAMETER ESTIMATION TECHNIQUES FOR DETERMINING SAFE VEHICLE  
SPEEDS IN UGVs

Dustin L. Edwards

Master of Science, May 10, 2008  
(B.S.M.E., Auburn University, 2005)

125 Typed Pages

Directed by David M. Bevly

This thesis develops simplified equations to predict a velocity in which vehicle rollover or tire saturation occur. These equations are functions of different vehicle parameters that are important to vehicle handling characteristics. Therefore, various algorithms are developed to estimate parameters such as vehicle tire stiffness, peak tire force, and center of gravity position on-line. A number of vehicle control systems have been developed in order to reduce rollover and help maintain vehicle stability. However, many of these control systems do not take into account changing vehicle parameters. Therefore using the on-line estimates of these parameters, the control systems could be more effective in decreasing the number of vehicle accidents.

The thesis first explains the fundamentals of lateral vehicle dynamics. Basic vehicle dynamic models are derived and validated to show the effectiveness and shortcomings of the different models. Many assumptions are used to simplify the

models. The assumptions lead to simplified equations that predict a velocity in which vehicle rollover or tire saturation occur. An equation to predict the vehicle stopping distance is also derived. Experiments are run to control the vehicle speed to the predictive velocity. This velocity is updated with the identified parameters from the estimation algorithms. By providing the updated velocity to the steering controller, a vehicle is able to transverse a maneuver at a safe speed.

## ACKNOWLEDGMENTS

Without the love and support from many friends and my family, this thesis would have been an impossible project. First and foremost, I must give thanks to God who has always been there for me during good and bad times. He has also blessed me and given me everything and everyone I have needed to succeed.

I would also like to thank my parents for the all the continuing support that they have given me during the last 26 years. They have taught me many things growing up including hard work, determination, and many other values. I would also like to thank my brother and sister for always being there for me when I needed them.

I would like to thank my graduate advisor, Dr. Bevly. He has continually challenged me throughout my college career and provided technical and financial support needed to make this thesis possible. And a special thanks to all those in the GPS and Vehicle Dynamics Lab who have helped me with the many questions I have asked during my research.

Finally, I would like to thank my best friend and wife, Jenny, who has given me all the love and support needed over the last two and a half years. I will be forever indebted to her for the sacrifices she has made during the completion of my graduate work.

Style manual or journal used Journal of Approximation Theory (together with the style known as “aums”). Bibliography follows the IEEE Transactions format.

Computer software used The document preparation package T<sub>E</sub>X (specifically L<sup>A</sup>T<sub>E</sub>X) together with the departmental style-file aums.sty.



## TABLE OF CONTENTS

	LIST OF FIGURES	xii
1	INTRODUCTION	1
1.1	Motivation . . . . .	2
1.2	Background and Literature Review . . . . .	4
1.3	Contributions . . . . .	6
1.4	Contributions . . . . .	7
1.5	Thesis Organization . . . . .	8
2	VEHICLE MODELING	9
2.1	Introduction . . . . .	9
2.2	Lateral Kinematic Model . . . . .	10
2.3	Lateral Bicycle Model . . . . .	12
2.4	Understeer Gradient . . . . .	15
2.4.1	Neutral Steer . . . . .	16
2.4.2	Understeer . . . . .	17
2.4.3	Oversteer . . . . .	17
2.5	Tire Models . . . . .	17
2.5.1	Fiala Tire Model . . . . .	20
2.5.2	Dugoff Tire Model . . . . .	22
2.6	Roll Model . . . . .	23
2.7	Vehicle Model Validation . . . . .	26
2.8	Conclusions on Vehicle Modeling . . . . .	31
3	PREDICTIVE VELOCITY CALCULATIONS	32
3.1	Introduction . . . . .	32
3.2	Predictive Velocity . . . . .	32
3.2.1	Zero-Sideslip Velocity . . . . .	33
3.2.2	Dugoff Velocity . . . . .	34
3.2.3	Rollover Velocity . . . . .	36
3.3	Stopping / Following Distance . . . . .	38
3.4	Experiments . . . . .	42
3.4.1	Dugoff Velocity . . . . .	42
3.4.2	Rollover Equation . . . . .	45
3.4.3	Stopping Distance . . . . .	45

3.5	Conclusions . . . . .	47
4	ESTIMATION ALGORITHM DEVELOPMENT	48
4.1	Introduction . . . . .	48
4.2	Tire Parameter Estimates . . . . .	49
4.2.1	Tire Stiffness and Peak Tire Force Estimation with Dugoff's Tire Model . . . . .	52
4.2.2	Estimation with Fiala's Tire Model . . . . .	55
4.3	Weight Split Estimation . . . . .	58
4.4	CG Height Estimation . . . . .	61
4.5	Experiments and Validation of Estimation Algorithms . . . . .	64
4.5.1	Experimental Setup . . . . .	64
4.5.2	Tire Parameter Estimation Experiments . . . . .	64
4.5.3	Weight Split Estimation Experiments . . . . .	74
4.5.4	CG Height Estimate Experiments . . . . .	76
4.6	Conclusion . . . . .	79
5	UPDATED PREDICTIVE VELOCITY EXPERIMENTS	80
5.1	Introduction . . . . .	80
5.2	Critical Velocity with Parameter Updates . . . . .	80
5.2.1	Zero Sideslip Velocity . . . . .	81
5.2.2	Dugoff Velocity . . . . .	85
5.2.3	Rollover Velocity . . . . .	89
5.3	Conclusions . . . . .	91
6	CONCLUSIONS	93
6.1	Overall Contributions . . . . .	93
6.2	Limitations . . . . .	94
6.3	Recommendations for Future Work . . . . .	94
	BIBLIOGRAPHY	96
	APPENDICES	100
A	VEHICLE NOMENCLATURE	101
B	VEHICLE PROPERTIES	103
C	TIRE PARAMETER AND WEIGHT SPLIT ESTIMATES USING DATA FROM CARSIM	105
C.1	Tire Parameter Estimator Validation with Carsim's G35 Sedan . . .	105

C.1.1	Tire Parameter Estimator Testing during Lateral Maneuver	105
C.1.2	Tire Parameter Estimator Testing during Longitudinal Ma- neuver . . . . .	107
C.2	Weight Split Estimator Validation with Carsim's G35 Sedan . . . .	109

## LIST OF FIGURES

2.1	Vehicle coordinates defined by the SAE [22] . . . . .	10
2.2	Kinematic Bicycle Model . . . . .	11
2.3	Bicycle Model FBD . . . . .	13
2.4	Basic Understeer Gradient Plot . . . . .	16
2.5	Generic Tire Curve . . . . .	18
2.6	Circle of Friction for Tire Forces . . . . .	19
2.7	Vehicle Roll FBD . . . . .	24
2.8	Comparison of the Kinematic and Bicycle Model during Slow-Speed Turning in the G35 Sedan . . . . .	27
2.9	Comparison of the Kinematic and Bicycle Model during High-Speed Cornering in the G35 Sedan . . . . .	28
2.10	Comparison of the Bicycle Model with Linear and Non-linear Tire Models during High-Speed Sliding Experiments in the G35 Sedan . . . . .	29
2.11	Roll Plane Model Validation of a Double Lane Change Maneuver in Carsim . . . . .	30
3.1	Roll Equation FBD . . . . .	37
3.2	Safe Following Distance . . . . .	38
3.3	Longitudinal Free Body Diagram . . . . .	39
3.4	Predicting Slidout at Radius of 152.5 and 400 meters with the Dugoff Velocity Equation . . . . .	43
3.5	Predicting Slidout at Radius of 152.5 and 400 meters with the new Dugoff Velocity Equation . . . . .	44

4.1	Tire Force Estimates . . . . .	51
4.2	Lateral Experimental Data in the G35 Sedan used in the Tire Parameter Estimator [8] . . . . .	69
4.3	Lateral Tire Stiffness and Peak Tire Force Estimate from G35 Data during a Lateral Slalom [8] . . . . .	70
4.4	Longitudinal Acceleration in the G35 Sedan used in the Tire Estimator [8] . . . . .	71
4.5	Longitudinal Stiffness and Peak Tire force Estimate from G35 Data during Acceleration and Braking[8] . . . . .	72
4.6	Accelerations and Yaw Rate Measurements for the Combined Lateral/Longitudinal Estimation [8] . . . . .	73
4.7	Tire Stiffness and Peak Tire Force Estimate during Lateral and Longitudinal Excitation of the G35 Sedan [8] . . . . .	74
4.8	Cornering Data in the G35 Sedan at NCAT Test Track . . . . .	75
4.9	Weight Split, $I_z$ Estimate During Cornering in the G35 Sedan . . . . .	76
4.10	Double Lane Change with Added Noise in Carsim’s Large SUV . . . . .	77
4.11	RLS Estimation of Large SUV’s CG Height, Roll Damping, and Roll Mass Moment of Inertia during a Double Lane Change in Carsim . . . . .	78
5.1	Desired Path for Vehicle Controlled at Zero Sideslip Velocity . . . . .	82
5.2	Weight Split Estimate in a Lane Change Maneuver at Zero Sideslip Velocity . . . . .	83
5.3	True and Desired Velocity Calculated from the Zero Sideslip Velocity in a Lane Change Maneuver in Carsim . . . . .	84
5.4	Sideslip with and without Desired Updated Velocity . . . . .	85
5.5	Coefficient of Friction Update during 400 Meter Radius Curve in Carsim’s G35 Sedan . . . . .	86

5.6	True and Desired Velocity Calculated from the Dugoff Velocity in a 400 m Radius turn in Carsim . . . . .	87
5.7	Tire Slip Angles in a 400 m Radius Turn with a Drop in Road Friction Coefficient while Controlling Speed at the Dugoff Velocity .	88
5.8	Estimated CG Height during a 400 m Radius Turn using data from Carsim's Large SUV . . . . .	90
5.9	True and Desired Velocity Calculated from the Rollover Velocity in a 200 m Radius turn in Carsim . . . . .	91
C.1	Slalom in Carsim's G35 Sedan . . . . .	106
C.2	Estimation of Tire Parameters during Slalom Maneuver . . . . .	107
C.3	Acceleration / Braking in Carsim's G35 Sedan . . . . .	108
C.4	Estimation of Tire Parameters during Acceleration / Braking Maneuver . . . . .	109
C.5	Double Lane Change with Added Noise in Carsim . . . . .	110
C.6	Weight Split, $I_z$ Estimate . . . . .	111

## CHAPTER 1

### INTRODUCTION

This thesis develops simplified equations to predict a velocity in which vehicle rollover or tire saturation occur. These equations are functions of different vehicle parameters that are important to vehicle handling characteristics. Therefore, various algorithms are developed to estimate parameters such as vehicle tire stiffness, peak tire force, and center of gravity position on-line. A number of vehicle control systems have been developed in order to reduce rollover and help maintain vehicle stability. However, many of these control systems do not take into account changes in the vehicle parameters. Therefore using the on-line estimates of these parameters, the control systems could be more effective in decreasing the number of vehicle accidents.

The thesis first explains the fundamentals of lateral vehicle dynamics. Basic vehicle dynamic models are derived and validated to show the effectiveness and shortcomings of the different models. Many assumptions are used to simplify the models. The assumptions lead to simplified equations that predict a velocity in which vehicle rollover or tire saturation occur. An equation to predict the vehicle stopping distance is also derived. Experiments are conducted to control the vehicle speed to the predictive velocity. This velocity is updated with the identified parameters from the estimation algorithms. By providing the updated

velocity to the speed controller, a vehicle is able to transverse a maneuver at a safe velocity.

## 1.1 Motivation

With an increase of vehicles on the road, vehicle safety is becoming more important each day. Considerable work has been conducted in the past to decrease the number of vehicle collisions. There is also a rising demand in research of autonomous vehicles. With a rising demand of autonomous vehicles and an increase of emphasis on vehicle safety, many different vehicle controls systems have been developed and implemented in today's cars to assist vehicle safety development. However, many of these control systems do not take into account changing vehicle parameters. With knowledge of important vehicle parameters, these control systems could be more effective in decreasing the number of vehicle crashes.

Electronic Stability Control (ESC) is one control method to help reduce the numbers of crashes on the road. It limits the lateral acceleration, yaw rate, or sideslip angle by individual wheel braking, steering input, etc. With the results of early ESC system, NHTSA has required ESC to be installed in all new vehicles by the 2012 model year [21]. The limits on the ESC systems are generally constant, however the ESC systems could possibly be improved by updating these limits based off of important vehicle parameters. When vehicle parameters change, so does the handling of the car. By taking the changing parameters into account when setting the ESC limits, the system should show improvement.



Many of the active safety systems also need a measurement of sideslip. This state has proven to be very difficult to estimate. Many researchers have developed methods to obtain this state using different sensors and estimators. While most sensors are too expensive to incorporate into every vehicle, one method integrates noisy and biased sensors to estimate this state [15]. Other researchers have used model based estimators along with inertial sensors to estimate sideslip [10]. For methods that used model based estimators to provide an estimate of the states, vehicle parameters must be known for these systems to provide an accurate estimate. This thesis presents different methods to estimate critical vehicle parameters that could be used to update vehicle parameters in different model based state estimators.

In addition to possibly providing estimated parameters for better accuracy of vehicle control systems and model based estimators, this thesis also presents a method to determine safe vehicle speed before it enters a tough maneuver. To accomplish this, critical velocity equations are developed to provide a safe speed to enter a turn. The value of speed calculated is then sent to the vehicle's control system as the maximum speed. Because the vehicle's handling depends on certain vehicle parameters, estimates from the parameter estimation algorithms are sent to update the critical velocity equations. By controlling the vehicle speed below a calculated maximum speed, the vehicle will likely already be under the ESC limits when it gets into the maneuver.

## 1.2 Background and Literature Review

Because vehicle safety is so important, many researchers have developed different methods to increase the vehicle's safety performance. However, many of these methods rely on accurate vehicle parameters to perform satisfactory. Recently, researchers studied the effects different vehicle parameters had on ESC systems [21]. This study proved that different center of gravity positions could effect the performance of the ESC systems and may not always prevent rollover or keep the vehicle sliding off the road. For this reason, many researchers have studied methods to estimate these critical parameters.

Since many lateral stability control systems need a measurement of sideslip, there has been much work done in this field. Many systems to estimate this state use model based estimators. For these to be successful, it is important for the vehicle parameters to be accurate. One researcher used estimates of tire cornering stiffness to improve estimation of vehicle states in a model based estimator [1]. Ryu proposed a method to estimate vehicle parameters that could be used for model based state estimation during periods of GPS outages [30]. When GPS signals are available, a simple kinematic filter could be used to update the states and also estimate important vehicle parameters [30]. When the GPS signal is lost, a model based approach is used to estimate the vehicle states, in which the estimated parameters are used in the model. This thesis develops methods to estimate these needed parameters.

Many methods have also been developed to estimate different vehicle properties. Recent work has estimated different tire properties. While some researcher have used lateral vehicle models to achieve an estimate of tire cornering stiffness [30, 32], others have used lateral vehicle models along with non-linear tire models to estimate cornering stiffness and tire road friction simultaneously [6, 16]. Other methods developed by researchers include measurements of the steering wheel torque to achieve estimates of these two important parameters [17, 20, 23]. By using a non-linear tire model that takes into account both lateral and longitudinal tire models, a method to estimate both the lateral and longitudinal tire stiffness, as well as peak tire force has been developed, previously published in [8]. By using this method, the peak tire force can be estimated during periods of longitudinal or lateral force generation providing more opportunity to estimate the tire parameters. By knowing these parameters, it is possible to have a better understanding of the vehicle's limits and provides many uses to further increase safety in today's automobiles.

Other important parameters that a vehicle's control system should take into account include the vehicle's center of gravity, as this heavily influences rollover and other handling aspects of the vehicle. Past researchers have developed methods to estimate this parameter. For example, one researcher developed a method that uses multiple models and switching to estimate the vehicle's CG position[33, 34]. One estimator, previously published in [9], uses a non-linear estimator to estimate

the lateral CG position [9]. To estimate the height of the center of gravity, a recursive least squares algorithm can be used.

### 1.3 Contributions

Since vehicle parameters heavily effect the handling and limits of an automobile, they must be taken into account to maximize safety of the vehicle control systems. This research attempts to develop different methods to obtain important vehicle parameters on-line and in real-time. By studying different vehicle models, it is apparent these parameters can be estimated with current sensors. This research develops a method to obtain estimates of peak tire force and lateral and longitudinal tire stiffness in either a longitudinal or lateral maneuver. This will greatly increase the chances of obtaining an estimate of the peak tire force, which highly effects when the vehicle may slide off the road. This thesis also develops a method to estimate the vehicle's CG position.

To help increase the safety of regular and autonomous vehicles, a method is introduced to limit the vehicle's velocity during certain driving maneuvers. This method uses predictive velocities, calculated from simplified vehicle models, to warn the driver or even update the controlled velocity in autonomous vehicles. These predictive velocities are based off parameters that mostly influence the handling characteristics of the vehicle. When a parameter changes, the parameter estimation algorithms will recognize this and update the predictive velocity with a new value. This will help the vehicle's controllers by limiting the speed of the

vehicle before the turn instead of trying to limit it when the vehicle has already reached the ESC limits. In summary, this thesis will attempt to assist current vehicle safety technology by providing the control system with estimated vehicle parameters on-line and also providing a max speed in which vehicle failure is eminent.

#### **1.4 Contributions**

This thesis develops methods to estimate critical vehicle parameters using model based estimators. The estimated parameters are then used to determine a safe traveling speed for the vehicle. In development of the algorithms, the following contributions were performed:

- An estimator was developed to estimate peak tire force and tire stiffness during lateral, longitudinal, and combined tire force generation increasing the chances of getting an estimate of these parameters.
- A method was developed to estimate the vehicles center of gravity position using an Extended Kalman Filter (EKF)
- A simplified velocity equation was derived to predict tire saturation.
- Predictive velocity equations and parameter estimation algorithms were used in conjunction to send a desired velocity to the speed controller, creating a safe traveling speed for the vehicle.

## 1.5 Thesis Organization

The remaining chapters in this thesis are organized as follows:

**Chapter 2** Vehicle Modeling. Chapter 2 will lay out the basic vehicle models used to estimate important vehicle parameters in this thesis. Validation plots are presented to show the effectiveness and shortcomings of the different models.

**Chapter 3** Critical Velocity Calculations. In Chapter 3, certain assumptions are made to the vehicle models to simplify them. From the simplifications, critical velocity equations are derived to minimize the sideslip, predict rollover, and to prevent the tire from sliding.

**Chapter 4** Estimation Algorithm Development. Chapter 4 develops methods to estimate parameters that effect vehicle rollover and sliding. The algorithms are then validated in simulation.

**Chapter 5** Experiments and Validation. Chapter 5 is devoted to testing and validation of the algorithms developed in Chapters 3 and 4. The critical velocities are updated with the parameter estimates and sent to the velocity controller. By using the critical velocities in different scenarios, the vehicle control system is supplied with a safe speed to enter a turn or lane change.

**Chapter 6** Conclusions. Chapter 6 will discuss the contributions and findings of this work. Some suggestions on future work will also be discussed.

## CHAPTER 2

### VEHICLE MODELING

#### 2.1 Introduction

In order to develop parameter estimation schemes for controller updates, accurate vehicle models must be developed. Vehicle models are the primary source of understanding vehicle dynamics. In this chapter, vehicle models are developed and studied in depth to fully understand how the vehicle reacts to different vehicle inputs. The coordinate system used in this thesis is defined by the Society of Automotive Engineers (SAE) and is shown in Figure 2.1. This coordinate system defines the longitudinal axis of the vehicle as  $x'$ , the lateral axis to be  $y'$ , and the vertical axis,  $z'$ , points toward the ground. The coordinate system also defines the direction of roll rate  $p'$ , pitch rate  $q'$ , and yaw rate  $r'$ . All models in this chapter will be based off the basic "bicycle model." Other models are developed to capture dynamics the bicycle model is unable to describe. Also, simplifications are made to the bicycle model that is valid during certain steady-state maneuvers. The models developed in this chapter is important in later sections when developing parameter estimation algorithms. Therefore, it is important to know the limitations and accuracy of each model. The nomenclature used in this chapter can be viewed in Appendix A.

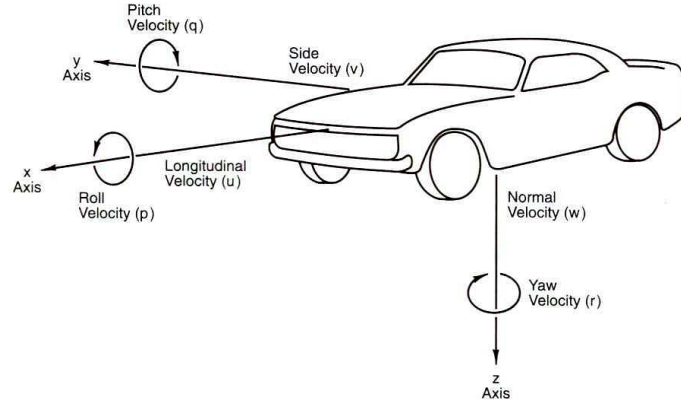


Figure 2.1: Vehicle coordinates defined by the SAE [22]

## 2.2 Lateral Kinematic Model

Under certain assumptions, lateral motion of a vehicle can be described by certain geometric relationships. These relationships allow for a mathematical description of the vehicle motion during certain maneuvers. One downside to this model is the relationships are very simplistic and may produce large errors from that of the true states during dynamic maneuvers. However, the relationships described below are very helpful in understanding the lateral motions of a vehicle.

To derive the kinematic relationships of the vehicle, consider the free body diagram (FBD) shown in Figure 2.2. One assumption of the bicycle model is the inner and outer tires are represented by one tire at the center of the vehicle's axle. This is true for both the front and rear axle. The steering angle of the vehicle is represented by  $\delta$ . The slip angle of the vehicle is denoted as  $\beta$  and describes the angle between the velocity vector and the longitudinal axis of the vehicle. For



this section, the slip angle and steer angle are assumed to be small. By neglecting slip angles at the tires, the velocity vector at each tire is assumed to be in the direction of the respective tire. Note that these assumptions are reasonable for vehicles traveling at slower speeds.

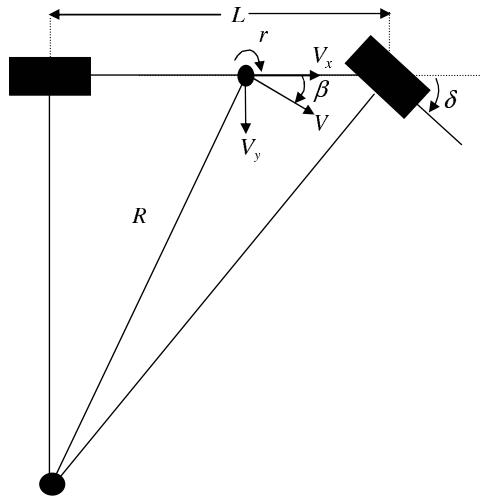


Figure 2.2: Kinematic Bicycle Model

At low speeds with no lateral tire slip, it can be shown that the perpendicular line from each tire passes through the same point which is called the center of the turn. If the steering angle of the front tire reaches zero, the radius of curvature ( $R$ ) goes to infinity. If the front wheels are not zero the steering angle can be described by Equation (2.1), known as the Ackerman Angle.

$$\delta = \tan^{-1} \left( \frac{L}{R} \right) \approx \left( \frac{L}{R} \right) \quad (2.1)$$

By using simple kinematics, the vehicle's velocity ( $V$ ) can be described as the yaw rate ( $r$ ) of the vehicle times the radius of curvature ( $R$ ). Also with no lateral sliding, the lateral acceleration,  $a_y$ , of the vehicle is simply the centripetal acceleration developed during the turn.

$$V = Rr \tag{2.2}$$

$$a_y = \dot{V}_y = Rr^2 = \frac{V^2}{R} = Vr \tag{2.3}$$

Substituting Equation (2.2) into (2.1) results in the expected yaw rate of the kinematic model, given a steer input and velocity.

$$r = \left(\frac{V}{L}\right) \tan(\delta) \approx \left(\frac{V}{L}\right) \delta \tag{2.4}$$

### 2.3 Lateral Bicycle Model

The Bicycle Model is used widely in vehicle dynamics to mathematically describe the motion of a vehicle [12, 29, 22] . It is a simple yet accurate way to estimate lateral vehicle states for vehicles that develop small roll angles. This model neglects pitch, weight transfer, and, in this section, longitudinal dynamics.

Another important, although accurate, assumption is the inner and outer slip angles and steer angles are lumped into one tire at the center of the axle similar to the previous model.

To show a visual picture of the bicycle model, a free body diagram is shown in Figure 2.3. The front and rear tire slip angles are denoted as  $\alpha_f$  and  $\alpha_r$  respectively. By summing the forces and moments on the free body diagram, a simple set of dynamic equations can be derived to describe the vehicle's lateral motion.

$$\Sigma F_y = m\ddot{y} = F_{yF} + F_{yR} \quad (2.5)$$

$$\Sigma M = I_z\dot{\psi} = aF_{yF} + bF_{yR} \quad (2.6)$$

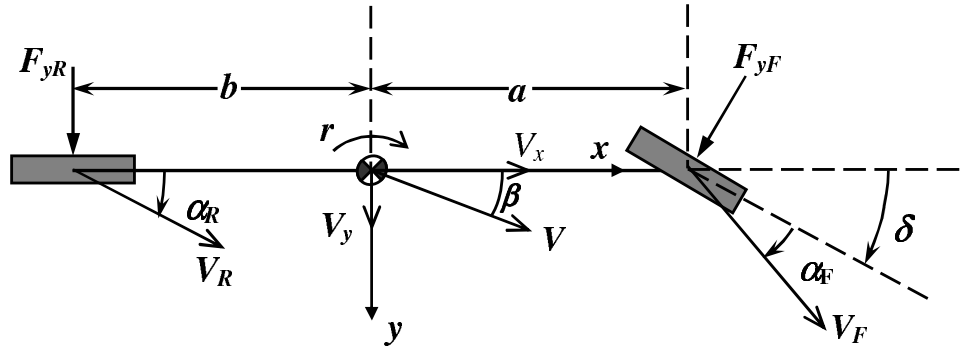


Figure 2.3: Bicycle Model FBD

To describe the front and rear tire forces ( $F_{yF,R}$ ), a linear tire model will be used. This model assumes the tire forces remain in the linear region of the tire and are proportional to the tire's respective slip angle times the tire's cornering stiffness ( $C_\alpha$ ), shown in Equation (2.7) and (2.8).

$$F_{yF} = -C_{\alpha f}\alpha_f \quad (2.7)$$

$$F_{yR} = -C_{\alpha r}\alpha_r \quad (2.8)$$

Because the tire sometimes leaves the linear region, more information on non-linear tire modeling will be presented in a later section.

Substituting Equations (2.7) and (2.8) into (2.5) and (2.6), a state space representation of this model can be developed shown by Equation (2.9).

$$\begin{bmatrix} a_y \\ \dot{r} \end{bmatrix} = \begin{bmatrix} -\frac{C_0}{mV_x} & -\frac{C_1}{mV_x} \\ -\frac{C_1}{I_zV_x} & -\frac{C_2}{I_zV_x} \end{bmatrix} \begin{bmatrix} V_y \\ r \end{bmatrix} + \begin{bmatrix} \frac{C_{\alpha f}}{m} \\ \frac{C_{\alpha f}}{I_z} \end{bmatrix} \delta \quad (2.9)$$

where,

$$\begin{aligned} C_0 &= C_{\alpha f} + C_{\alpha r} \\ C_1 &= aC_{\alpha f} - bC_{\alpha r} \\ C_2 &= a^2C_{\alpha f} + b^2C_{\alpha r} \end{aligned} \quad (2.10)$$

With a state space representation, this model can be configured for control or estimation purposes.

In order to calculate the steady state tire slip, Equations (2.5) and (2.6) are simplified by assuming yaw acceleration is equal to zero and lateral acceleration is equal to the centripetal acceleration shown by Equation (2.3). This results in the following simplified equations for the lateral tire forces.

$$m \frac{V^2}{R} = F_{yF} + F_{yR} \quad (2.11)$$

$$0 = aF_{yF} + bF_{yR} \quad (2.12)$$

Substituting Equations (2.7-2.8) into the above equations, the steady-state tire slip can be solved. This results in Equations (2.13-2.14).

$$\alpha_f = \frac{W_f V^2}{C_{\alpha f} g R} \quad (2.13)$$

$$\alpha_r = \frac{W_r V^2}{C_{\alpha r} g R} \quad (2.14)$$

## 2.4 Understeer Gradient

In order to develop a better understand of the turning response of a vehicle, the understeer gradient of the vehicle is defined. Using the steady-state bicycle model, the understeer gradient can be determined from the weight distribution and the cornering stiffness [30]. By including slip angles into Figure 2.2, a simple kinematic equation between the steer angle and tire slip angles can be developed.

$$\delta \approx \frac{L}{R} + \alpha_f - \alpha_r \quad (2.15)$$

Substituting Equations (2.13 - 2.14) into the above equation gives:

$$\delta \approx \frac{L}{R} + \left( \frac{W_f}{C_{\alpha f}} - \frac{W_r}{C_{\alpha r}} \right) \frac{V^2}{gR} \approx \frac{L}{R} + K_{us} a_y \quad (2.16)$$

From the above equation, the understeer gradient is labeled as  $K_{us}$ . The understeer gradient determines both the magnitude and the direction of the steering inputs required for a given lateral acceleration [12]. The understeer gradient also determines if the vehicle is neutral steer, oversteer, or understeer. Figure 2.4 shows the basic principles with  $K_{us}$  being the slope of each line.

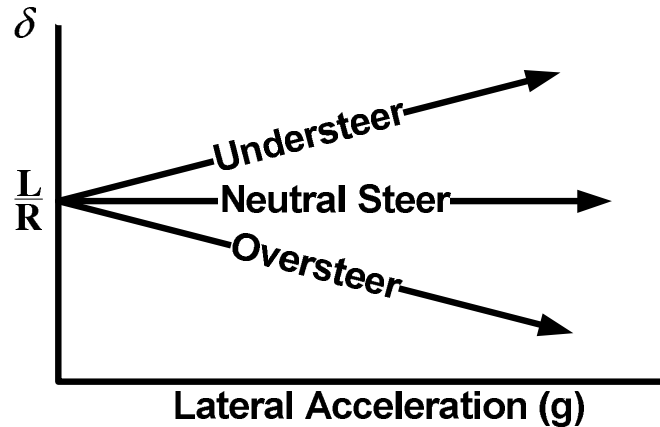


Figure 2.4: Basic Understeer Gradient Plot

#### 2.4.1 Neutral Steer

Neutral steer occurs when the understeer gradient is zero, which results in the front and rear steady state tire slip angles being equivalent. By studying

Equation (2.16), during neutral steer the steer angle required to make the turn is approximately the Ackerman angle.

### 2.4.2 Understeer

Understeer occurs when  $K_{us}$  is greater than zero causing larger slip angles to develop in the front tire than the rear. Because there is more slip at the front tire, the steer angle must increase to maintain the radius of the curve. During this condition, the steer angle increases linearly with the speed squared or the lateral acceleration.

### 2.4.3 Oversteer

Oversteer is the opposite of understeer. During oversteer,  $K_{us}$  is less than zero causing the rear tire slip angle to be greater than the front. Because the rear is sliding more than the front, less steer angle is required to navigate the turn.

## 2.5 Tire Models

With the exception of aerodynamic forces, all external forces on the vehicle are developed at the tire's contact patch. Therefore it is necessary to have full understanding of the relationship between the tire's contact patch and the surface the vehicle is on. The tire serves three basic functions:

- 1) It supports the vertical load, while cushioning against road shocks.
- 2) It develops longitudinal forces for acceleration and braking.

3) It develops lateral forces for cornering.

Figure 2.5 shows typical characteristics of a tire under lateral force generation modeled by the Fiala tire model. More information on this model will be discussed later. As shown in the plot, the lateral tire force remains linear with slip angle, as modeled by Equations (2.7) and (2.8), until the tire becomes saturated. This model relates peak tire force to the tire-road friction ( $\mu$ ) times the normal force ( $F_z$ ), known as the peak tire force. Therefore, the peak tire force increases with a rise in normal force. The longitudinal tire curve looks similar to the lateral tire model but instead is linear with the longitudinal tire slip. For this reason, it is very important to have an accurate estimate of  $\mu$  in order to reasonably predict the onset of sliding.

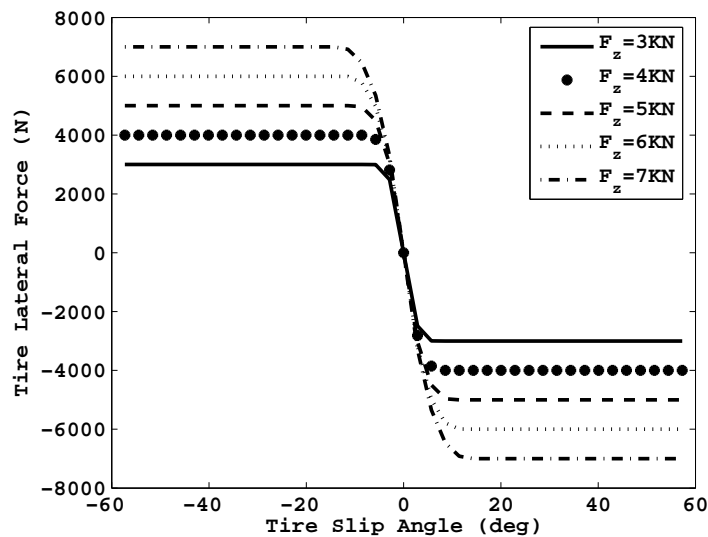


Figure 2.5: Generic Tire Curve



Vertical forces on the tire are not only important for ride characteristics, but also help to describe the max longitudinal and lateral forces developed by the tire. As shown in Figure 2.6, the magnitude of lateral and longitudinal tire force cannot exceed the peak tire force. When the magnitude of tire force reaches this point, sliding occurs. By studying the figure, it is obvious that the available drive force decreases with an increase in lateral force. Because of this effect, both forces must be taken into account during combined lateral and longitudinal tire force generation to develop an accurate vehicle model.

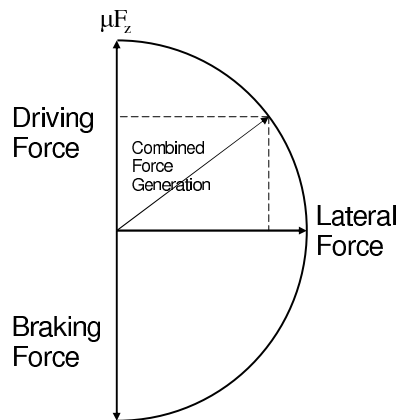


Figure 2.6: Circle of Friction for Tire Forces

Several researchers have developed models to describe the generated tire forces. One of the most well known models, called the Magic Formula tire model, was developed by Pacejka [27, 26, 25]. This model is an empirical formula capable of calculating lateral and longitudinal tire forces. Alternatively, the two models used in this paper are the Fiala and Dugoff tire model. Both models have their pros and cons and will be discussed in more detail below.

### 2.5.1 Fiala Tire Model

The Fiala tire model was originally developed to estimate lateral tire force generation only [11]. The model was however transformed to take into account both lateral and longitudinal forces [24]. One assumption to accomplish this transformation was lateral and longitudinal tire stiffness ( $C_\alpha, C_\sigma$ ) are equal. This is not always true however. The total slip ( $\sigma$ ) for this model is simply the magnitude of the lateral and longitudinal slip ( $\sigma_y, \sigma_x$ ), shown by Equation (2.17).

$$\sigma = \sqrt{\sigma_y^2 + \sigma_x^2} \quad (2.17)$$

To calculate the total slip, the individual values for slip must be known. Both the longitudinal and lateral slip are found using Equations (2.18) and (2.19) below.

$$\begin{aligned} \sigma_x &= \frac{r_{eff}\omega_w - V_x}{r_{eff}\omega_w} && \text{during acceleration} \\ \sigma_x &= \frac{r_{eff}\omega_w - V_x}{V_x} && \text{during braking} \end{aligned} \quad (2.18)$$

$$\sigma_y = \frac{V_x}{r_{eff}\omega_w} \tan(\alpha) \quad (2.19)$$

Both of these values may be calculated using different sensors described in Chapter 4. By assuming a parabolic pressure distribution on the tire's contact patch, Equation (2.20) is used to describe the magnitude of force on the tire, using the Fiala tire model.

$$F_t = \begin{cases} \mu F_z [3\theta\sigma - \frac{1}{3}(3\theta\sigma)^2 + \frac{1}{27}(3\theta\sigma)^3] & \text{if } \sigma \leq \sigma_m \\ F = \mu F_z & \text{if } \sigma \geq \sigma_m \end{cases} \quad (2.20)$$

The variable,  $\sigma_m$ , is the value of total slip where sliding occurs in the Fiala tire model. As described by the circle of friction, sliding is assumed to begin when the maximum tire force is equal to  $\mu F_z$ .

$$\sigma_m = \frac{1}{\theta} = \frac{3\mu F_z}{C_{\alpha/\sigma}} \quad (2.21)$$

The individual values of lateral and longitudinal tire force ( $F_y, F_x$ ) can be obtained by breaking up the force magnitude ( $F_t$ ). This is done by multiplying the force magnitude by the ratio of total slip to each forces respective slip, as shown in Equation (2.22) and (2.23).

$$F_x = \frac{\sigma_x}{\sigma} F \quad (2.22)$$

$$F_y = \frac{\sigma_y}{\sigma} F \quad (2.23)$$

In the case of pure lateral slip, set  $\sigma_y = \tan(\alpha)$  and  $\sigma_x = 0$  in the Fiala tire model. In case of pure longitudinal slip, set  $\sigma_y = 0$  [29]. By reducing the combined force generation model to either lateral or longitudinal force generation, simpler calculations can be obtained by reducing the amount of noisy measurements.

### 2.5.2 Dugoff Tire Model

The Dugoff model is similar to the Fiala model in that it allows for tire force estimates during combined tire force generation. The main difference is the Dugoff tire model assumes a uniform vertical pressure distribution on the tire's contact patch [7]. This is a simplification from the Fiala's tire model, but it allows for individual values of lateral and longitudinal tire stiffness which is shown to be advantageous in Chapter 4. The longitudinal and lateral tire forces are given by Equations (2.24) and (2.25), respectively.

$$F_x = C_\sigma \frac{\sigma_x}{1 + \sigma_x} f(\lambda) \quad (2.24)$$

$$F_y = C_\alpha \frac{\tan(\alpha)}{1 + \sigma_x} f(\lambda) \quad (2.25)$$

where,

$$\lambda = \frac{\mu F_z (1 + \sigma_x)}{2[(C_\sigma \sigma_x)^2 + (C_\alpha \tan(\alpha))^2]^{\frac{1}{2}}} \quad (2.26)$$

$$f(\lambda) = \begin{cases} (2 - \lambda)\lambda & \text{if } \lambda < 1 \\ 1 & \text{if } \lambda \geq 1 \end{cases} \quad (2.27)$$

Similar to the Fiala tire model, this model has a transition that occurs when  $\lambda = 1$ . This transition occurs when the tire leaves the linear region and begins the non-linear region. If the tire is experiencing lateral slip only, the model may be

reduced by setting  $\sigma_x = 0$  or for pure longitudinal force generation simply set  $\alpha = 0$ . This helps to simplify the model during driving conditions where only lateral or longitudinal forces are generated.

## 2.6 Roll Model

In this section, different vehicle roll models will be described and studied. It is very important to understand vehicle roll and rollover. Many researchers have developed models to describe the roll dynamics of vehicles during cornering. Some models are fairly simple while others are very in depth and require more parameters. The simpler roll models do not include the springs and dampers of the suspension and therefore assumes the sprung mass is stationary with the axle. Other high-fidelity models take into account forces produced by the springs and dampers.

In order to produce a reliable roll model, a free body diagram (FBD) must be developed. The FBD in Figure 2.7 shows a two state roll plane model [33, 34]. Three important parameters used in this model include the CG height ( $h_{cg}$ ), roll stiffness ( $K_\phi$ ), and roll damping coefficient ( $C_\phi$ ). This model lumps the entire vehicle mass into the sprung mass. This assumption allows a simplified equation for the spring and damper torques, shown in Equations (2.28-2.29).

$$T_{spring} = K_{\phi}\phi \quad (2.28)$$

$$T_{damper} = C_{\phi}\dot{\phi} \quad (2.29)$$

Notice that both equations also assume the spring and damper torques are linear with roll ( $\phi$ ) and roll rate ( $\dot{\phi}$ ), respectively.

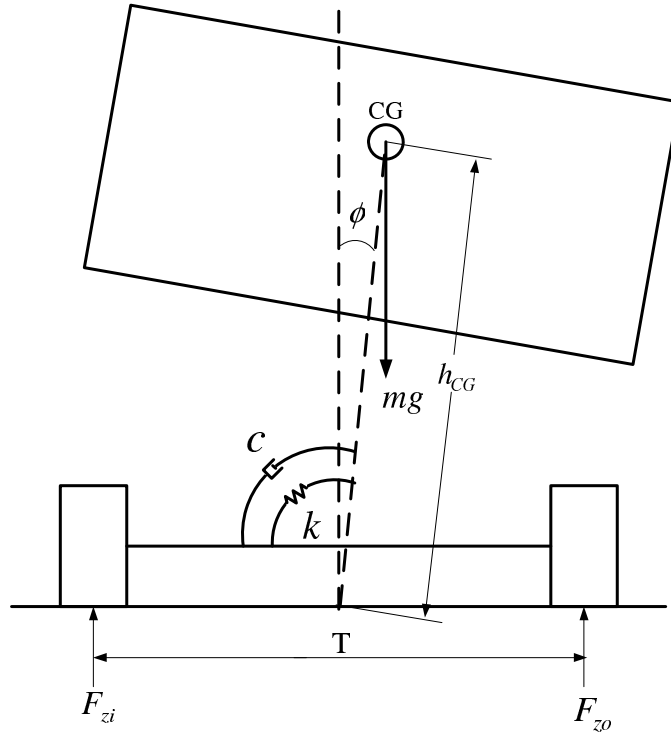


Figure 2.7: Vehicle Roll FBD

By summing the moments about the roll center on Figure 2.7, a simple equation is derived to describe the roll dynamics of the vehicle. Equation (2.30) assumes

the vehicle's sprung mass rotates about a fixed point at the centerline of the lateral axis on the ground.

$$J_{eff}\ddot{\phi} + C_{\phi}\dot{\phi} + K_{\phi}\phi = mh_{cg}(a_y\cos(\phi) + g\sin(\phi)) \quad (2.30)$$

By assuming a steady-state turn and small angles, Equation (2.30) can be simplified to solve for the roll angle with knowledge of the CG height and the spring roll stiffness.

$$\phi = \frac{mh_{cg}a_y}{K_{\phi} - mhg} = \frac{mh_{cg}V^2}{R(K_{\phi} - mh_{cg}g)} \quad (2.31)$$

Equation (2.30) may be transformed into a state space representation. The state space representation is shown in Equation (2.32).

$$\begin{bmatrix} \dot{\phi} \\ \ddot{\phi} \end{bmatrix} = \begin{bmatrix} 0 & 1 \\ -\frac{K_{\phi}-mgh_{cg}}{J_{eff}} & -\frac{C_{\phi}}{J_{eff}} \end{bmatrix} \begin{bmatrix} \phi \\ \dot{\phi} \end{bmatrix} + \begin{bmatrix} 0 \\ \frac{mh_{cg}}{J_{eff}} \end{bmatrix} a_y \quad (2.32)$$

Many other models have also been used to analyze roll dynamics. Some models developed do not assume the vehicle's roll center is located at ground height. One model assumes the roll center is not at ground level and the imaginary roll center also produces reactionary forces was developed in [36, 37].

## 2.7 Vehicle Model Validation

To show the accuracy and limitations of the models, each model is validated with experimental data. The data is from a G35 sedan at the National Center for Asphalt Technology (NCAT) test track. More details from the sensor implementation is discussed in Chapter 4. Carsim, a high-fidelity vehicle simulation software, is also used throughout this thesis.

With the data gathered at NCAT test track, the kinematic and bicycle model are validated in MATLAB. The parameter values used in the simulations of the G35 sedan is listed in Appendix B. By using MATLAB to simulate the dynamic equations presented in this chapter, Figure 2.8 shows that both the kinematic and bicycle model matches the recorded data at 2m/s, as would be expected. However for larger slip angles, the assumptions of the kinematic model break down causing the model to perform poorly. In the data logged at NCAT, slip angles remained small enough for both the bicycle and kinematic model to hold true. When vehicles reach higher speeds, as shown in the next experiment, the simplistic kinematic model is not the best choice.



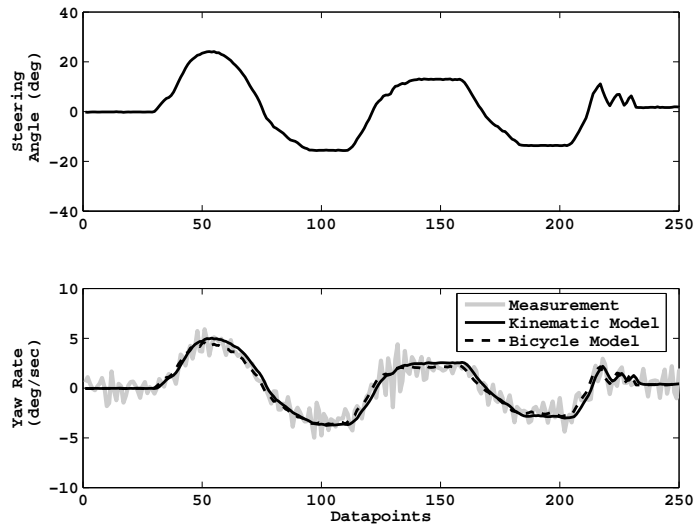


Figure 2.8: Comparison of the Kinematic and Bicycle Model during Slow-Speed Turning in the G35 Sedan

To show the shortcomings of the kinematic model, data was logged in a G35 sedan at higher speeds around NCAT test track. The inputs were run through both models in MATLAB and the results are shown in Figure 2.9. Notice the difference in the kinematic and bicycle models prediction of yaw rate. While cornering at high speeds with large slip angles, the kinematic model can not accurately predict the vehicle's dynamics.

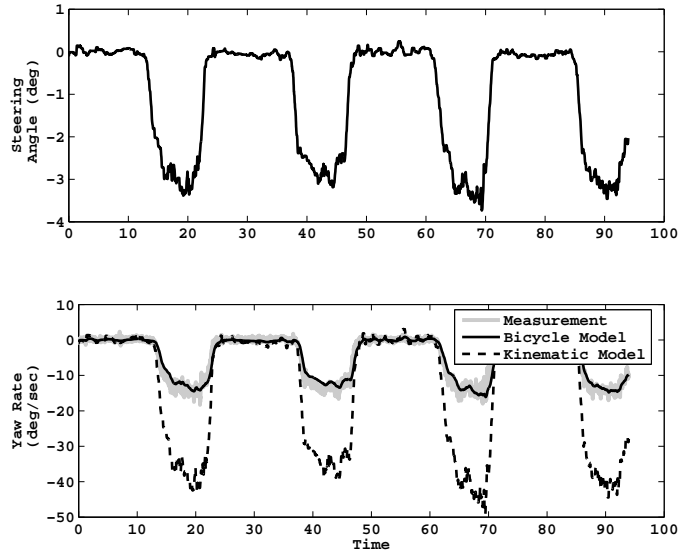


Figure 2.9: Comparison of the Kinematic and Bicycle Model during High-Speed Cornering in the G35 Sedan

To illustrate the shortcomings of the bicycle model with a linear tire model, a maneuver is conducted which saturates the tires enough for the vehicle to begin sliding. This is a very hard maneuver and is conducted to show a linear tire model without saturation can not describe the vehicle motion at the limits of handling. The more advanced model uses the Dugoff tire model to calculate the lateral tire forces. Figure 2.10 shows the bicycle model with a linear tire failing to match the data when the vehicle loses control. However, the bicycle model with a non-linear tire model matches the data fairly well, although there is still some mismatch at the highest peak. This is most likely due to the fact that the model does not take into account vehicle roll dynamics.

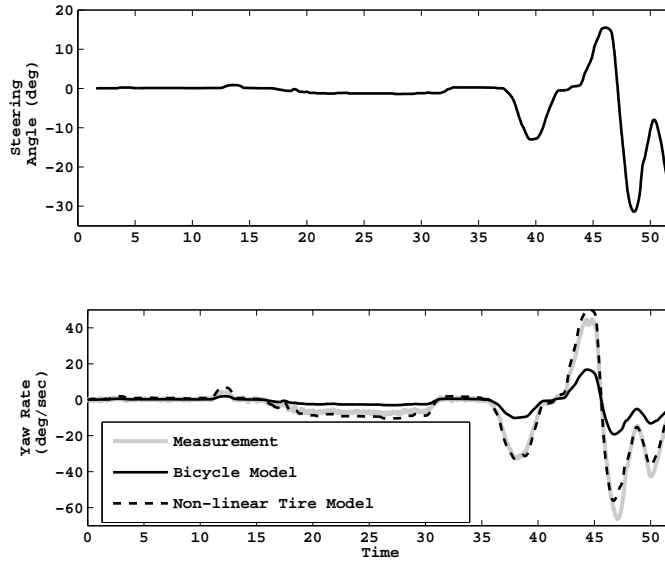


Figure 2.10: Comparison of the Bicycle Model with Linear and Non-linear Tire Models during High-Speed Sliding Experiments in the G35 Sedan

Finally, the two state roll plane model is tested. The vehicle used in this simulation is a large SUV from Carsim. Carsim is a high fidelity vehicle simulation tool that can be used to validate simplified vehicle models. Carsim is chosen in this experiment because a vehicle is needed that produces large roll angles, unlike the G35 sedan used in previous experiments. Appendix B provides the parameter values used in the roll plane model during this simulation. The large SUV attempts a double lane change in order to induce large roll rates and angles. The data from Carsim is used to compare with the simple two state roll plane model, which is simulated in MATLAB. The data from Carsim matches up well with the simple roll plane model, given in Equation (2.30), as shown in Figure 2.11.

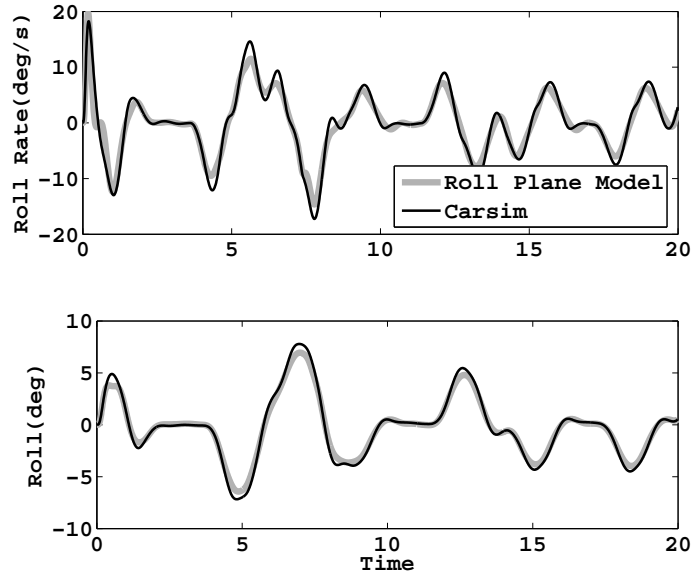


Figure 2.11: Roll Plane Model Validation of a Double Lane Change Maneuver in Carsim

One difference in this model and the Carsim high-fidelity model is the springs used in the Carsim model are highly non-linear. Shown by Equation (2.28), the simple roll plane model assumes linear springs. Now that the roll plane has been validated it can be used to estimate certain unknown parameters that may change such as the roll height. This parameter is important to know as it is one of the main factors in vehicle rollover [21].

## 2.8 Conclusions on Vehicle Modeling

In this chapter, vehicle models were developed and implemented into Matlab in order to develop a better understanding of vehicle dynamics. A simplistic kinematic model was developed and shown to match the vehicle dynamics at lower speeds in the Infiniti G35 sedan. For cornering at faster speeds, the kinematic lateral vehicle model failed to accurately describe this vehicle's dynamics. However, the bicycle model developed in Section 2.3 accurately described the vehicle's lateral motion. The pros and cons of using a linear tire model versus a non-linear tire model in the bicycle model was also discussed in this chapter. For modeling the roll dynamics of a vehicle, a simple roll plane model was derived. This model was validated with simulated data in Carsim from a large SUV. Carsim was used to provide a vehicle with a higher center of gravity position than the G35 sedan. Overall, this chapter showed the effectiveness of describing lateral and roll dynamics of a vehicle, while also describing the shortcomings of each models.

## CHAPTER 3

### PREDICTIVE VELOCITY CALCULATIONS

#### 3.1 Introduction

In this chapter, equations are derived to find a steady-state speed that a vehicle can safely transverse a curve. The velocities calculated take into account radius of curvature, rollover, small sideslip angles, and tire-road friction. Several assumptions are used to simplify equations of motion of the vehicle during different maneuvers. It is also assumed that the radius of curvature of the road is known from the path planner or a map database. These velocities are used in Chapter 5 to update the controlled velocity during different maneuvers. Also, a following distance is calculated for vehicles driving in platoons by taking into account the maximum braking forces available at the vehicle's tires. These equations could be beneficial to autonomous vehicles when traveling alone or in platoons by providing information about what speeds to travel or how far away to follow another vehicle.

#### 3.2 Predictive Velocity

In order to develop the equations discussed above, several assumptions are made. Many of the equations used in this section are based off a simplified version of the bicycle model. The simplified version of the the bicycle model assumes the vehicle is in steady-state. The steady state sideslip is then calculated. Both the

zero-sideslip and Dugoff velocity rely on the steady-state bicycle model. Similarly, the rollover velocity is derived from a simplification of the roll model. To view the nomenclature used in this chapter, view Appendix A.

### 3.2.1 Zero-Sideslip Velocity

With the lateral tire slip known at the tires, certain criteria is set to calculate a look-ahead velocity. One method used by Gillespie [12] is to find the velocity with zero sideslip at the vehicles center of gravity (CG). As discussed in Chapter 2, sideslip is simply the angle between the velocity vector and the vehicles longitudinal axis and can be calculated by Equation (3.1).

$$\beta = \alpha_r + \frac{b}{R} \quad (3.1)$$

To represent Equation (3.1) as a function of velocity, the above equation is combined with Equation (2.14). Then by setting the sideslip equal to zero, the zero sideslip velocity can be calculated with Equation (3.2).

$$V_{\beta=0} = \sqrt{bg \frac{C_{ar}}{W_r}} \quad (3.2)$$

The above equation provides for a safe speed in an autonomous vehicle during cornering or lane change maneuvers. However, this equation is not a function of

the turning radius and may provide speeds much lower than desired around larger radius turns. It also doesn't take into account the friction limits of the driving surface. Instead this velocity is a only function of the weight split and cornering stiffness.

### 3.2.2 Dugoff Velocity

In order to calculate a velocity based off tire-road friction and radius of curvature, the Dugoff tire model is used. This model was discussed more in depth in Chapter 2. The purpose of using this model is it has a transition when the tire leaves the tires circle of friction. The basic equations used in this subsection were described previously by Equations (2.24-2.26). However, for this section the Dugoff tire model is simplified to lateral force generation only. By making this assumption, the Dugoff tire model reduces down to the form shown in Equations (3.3-3.5).

$$F_y = C_\alpha \tan(\alpha) f(\lambda) \quad (3.3)$$

where,

$$\lambda = \frac{\mu F_z}{2C_\alpha \tan(\alpha)} \quad (3.4)$$

$$f(\lambda) = \begin{cases} (2 - \lambda)\lambda & \text{if } \lambda < 1 \\ 1 & \text{if } \lambda \geq 1 \end{cases} \quad (3.5)$$



Gunter and Sankar developed a friction circle interpretation of the Dugoff model [13]. It proves that if  $\lambda > 1$ , the tire's operation point is inside the friction circle and if  $\lambda \leq 1$ , the tires operation point is outside the friction circle. Since longitudinal dynamics are ignored, if the lateral tire force is less than the friction coefficient times the load on the tire, the tire remains in the circle of friction. This is used as the criteria to calculate a critical velocity from the Dugoff tire model. Assuming small angles, the non-equality equation, in Equation (3.6), is derived to keep the lateral tire force inside the friction circle assuming no longitudinal force generation and by setting  $\lambda = 1$  in Equation (3.4).

$$\frac{\mu F_z}{2C_\alpha \alpha} > 1 \quad (3.6)$$

Substituting Equation (2.13) into Equation (3.6), the velocity that ensures the tire remains inside the friction circle during steady-state turns can be calculated as shown below.

$$V_{Dug} < \sqrt{\frac{\mu Rg}{2}} \quad (3.7)$$

The above velocity can be easily determined if the radius of curvature and the friction coefficient is known. During turning around a large radius of curvature, this velocity would allow high speed turning without losing control or sliding

out. If the tire-road friction coefficient changes during the turn, the vehicle could however begin to slide out. For this reason, a method to estimate the road's friction coefficient will be developed in Chapter 4.

### **3.2.3 Rollover Velocity**

To provide safe speeds for any vehicle, rollover must be taken into account. This is especially true for vehicles with a high center of gravity, as these vehicles are more prone to rollover. Instead of sliding out like the above section describes, a larger vehicle tends to rollover. Many previous researchers have worked on rollover prediction formulas [28, 19, 14].

To obtain knowledge of when rollover will occur, a simple rollover prediction formula is developed previously discussed here [21]. Rollover can be defined as the point when all the vehicle's normal force is shifted to one side [21]. By neglecting the suspension effects, the vehicle can be modeled as a solid mass and transients from the suspension are ignored. A simple FBD in Figure 3.1 is used to describe this assumption.

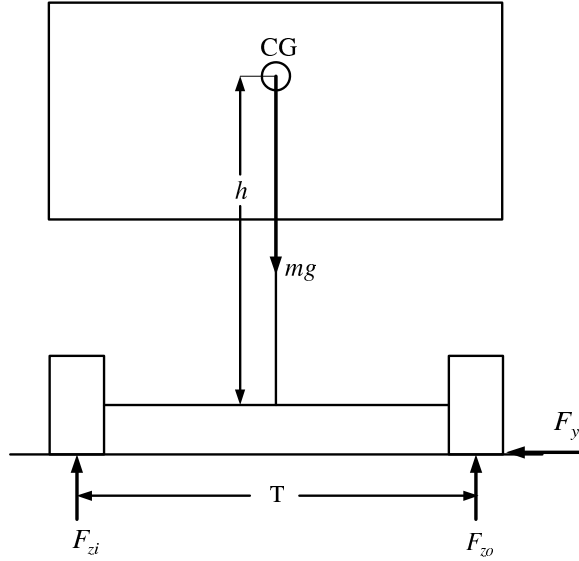


Figure 3.1: Roll Equation FBD

By summing the vertical and lateral forces as well as the moment on Figure 3.1, the following equations are developed.

$$\sum F_y = m * a_y = F_y \quad (3.8)$$

$$\sum F_z = ma_z = mg - F_z = 0 \quad (3.9)$$

$$\sum M_{CG} = \frac{T}{2}F_z - h_{cg}F_y = 0 \quad (3.10)$$

By simplifying the above equations, the rollover prediction formula is derived. This equation is widely used and is shown in Equation (3.11) [14, 12, 21].

$$V_{Rollover} = \frac{Tg}{2rh_{cg}} = \sqrt{\frac{TRg}{2h_{cg}}} \quad (3.11)$$

Lambert [21] recently developed a method to incorporate weight split and suspension effect into the rollover prediction formula. By studying trends in rollover data, a scale factor based on the understeer gradient of the vehicle was added to the formula to take into account weight split. An additional constant ( $\kappa$ ) for the suspension effects was also added as shown in the equation below.

$$V_{Rollover} = \kappa \frac{Tg}{2rh_{cg}}(1 + K_{us}) = \kappa \sqrt{\frac{TRg}{2h_c g}}(1 + K_{us}) \quad (3.12)$$

### 3.3 Stopping / Following Distance

In order for multiple vehicles to travel together in a fleet, a safe following distance must be known in order to prevent vehicle accidents. Figure 3.2 shows an example of a vehicle driving too close and a vehicle at a safe following distance. Note that the definition of "too close" is based on braking capability of the vehicle and the road surface.

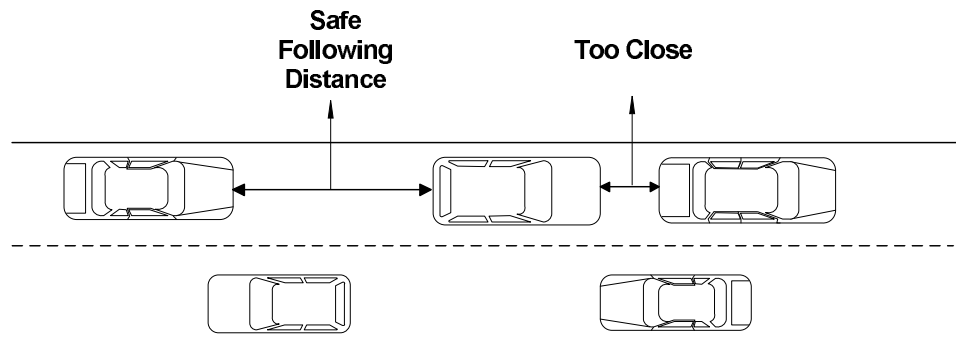


Figure 3.2: Safe Following Distance

For an autonomous vehicle in a fleet, a safe following distance provides many advantages over a vehicle without any knowledge of safe distance from the vehicle in front. Many sensors, such as a lidar, can provide a measurement of distance from one vehicle to the next for control purposes. If a safe following distance is known, rear-end collisions could be prevented.

In order to calculate a proper following distance, a simple longitudinal vehicle model is used. Figure 3.3 shows a very simplistic FBD of a longitudinal vehicle during braking. By summing the forces in the longitudinal direction, a simple equation is developed to describe the longitudinal motion of the vehicle.

$$\Sigma F_x = ma_x = -\text{External Forces} = -F_{xt} \quad (3.13)$$

Where  $F_{xt}$  is the braking force.

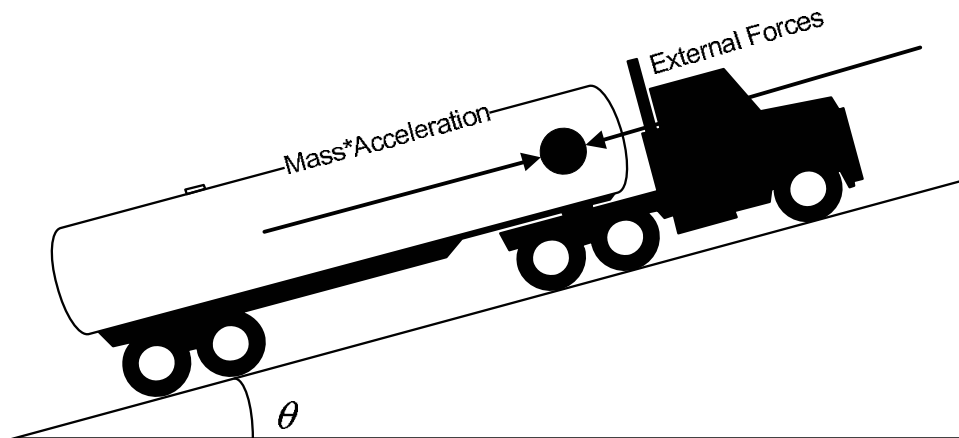


Figure 3.3: Longitudinal Free Body Diagram

In actuality, many forces effect the longitudinal dynamics, such as road slope, aerodynamic forces, braking and acceleration forces at the tire, and rolling resistance. However, to calculate a stopping distance, in this thesis some forces are ignored. When the equation is simplified to include only the braking force ( $F_{xt}$ ), the linear deacceleration ( $D_x$ ) can be described by Equation (3.14).

$$D_x = -\frac{dV}{dt} = \frac{F_{xt}}{m} \quad (3.14)$$

Assuming that the braking force is constant during the deacceleration, Equation (3.14) can be integrated to find the time ( $ts$ ) for a certain change in velocity [12].

$$ts = (V_o - V_F) \frac{m}{F_{xt}} \quad (3.15)$$

In order to solve for stopping distance, the relation  $dt = \frac{dx}{V}$  can be substituted into Equation (3.14) for dt. After integrating the equation and assuming the final velocity is zero, the stopping distance can be determined by Equation (3.16) [12].

$$SD = \frac{mV_o^2}{2F_{xt}} \quad (3.16)$$

The minimum stopping distance occurs when the braking force equals the peak longitudinal tire force, discussed in Chapter 2. Figure 2.6 shows that the max available braking force is equal to the friction coefficient times the normal force when neglecting lateral dynamics. By substituting  $\mu F_z$  in for  $F_{xt}$ , a final equation for stopping distance is created.

$$SD = \frac{mV_o^2}{2\mu F_z} = \frac{V_o^2}{2\mu g} \quad (3.17)$$

If the applied braking force to the tires is known, Equation (3.16) can be used to solve for the braking distance. However, if the braking force exceeds the peak tire force then Equation (3.17) must be used. This is because the tire-road interaction force can saturate and the tire slides at the peak tire force.

If the vehicle is stopping on a sloped road, the equation can be modified to take into account the road grade ( $\theta$ ). Assuming road grade and braking are the only external forces on the vehicle, the deceleration of the vehicle is described by Equation (3.18).

$$D_x = -\frac{dV}{dt} = \frac{F_{xt}}{m} + g \sin \theta \quad (3.18)$$

Assuming the road slope does not change with the distance, the relation  $dt = \frac{dx}{V}$  can be substituted into Equation (3.18). By integrating the above equation, a

stopping distance formula that depends on braking and road slope is developed, as shown in Equation (3.19).

$$SD = \frac{V_o^2}{2\left(\frac{F_{xt}}{m} + g\sin\theta\right)} = \frac{V_o^2}{2g(\mu + \sin\theta)} \quad (3.19)$$

By implementing this equation during travel on a hillside, a safer following distance will be possible, assuming the road slope is known or measured.

### 3.4 Experiments

To test the critical velocity and stopping distance equations, a series of tests were run in Carsim. These test were run to determine slideout, rollover, and stopping distance of a vehicle and how well the simplified equations match up to the values from a high fidelity simulation in Carsim. Parameters for the G35 sedan and the large SUV used in the following simulations are found in Appendix B. The G35 sedan is used in the Dugoff velocity and zero sideslip velocity simulations, while the rollover experiments are conducted with the large SUV.

#### 3.4.1 Dugoff Velocity

The Dugoff velocity is developed to keep the vehicle's tires inside the friction circle. It may also be noted that this equation does not take into account vehicle roll so during high amounts of roll the vehicle may slide out quicker than the value calculated from Equation (3.7).



To test the Dugoff velocity equation, two simulations were run in Carsim. The simulations consisted of a G35 sedan slowly accelerating around two circles, one with a radius of 152.4 meters and another with radius of 400 meters. The experiments consisted of four different simulations per circle. Each simulation had a different value for tire-road friction to fully test the equation's accuracy to predict a slide out. Figure 3.4 shows both the simulations with the asterisks being the Dugoff velocity calculated from the friction coefficient and the radius of curvature. Remember, this velocity is used to predict at what speed the tire reaches its limits.

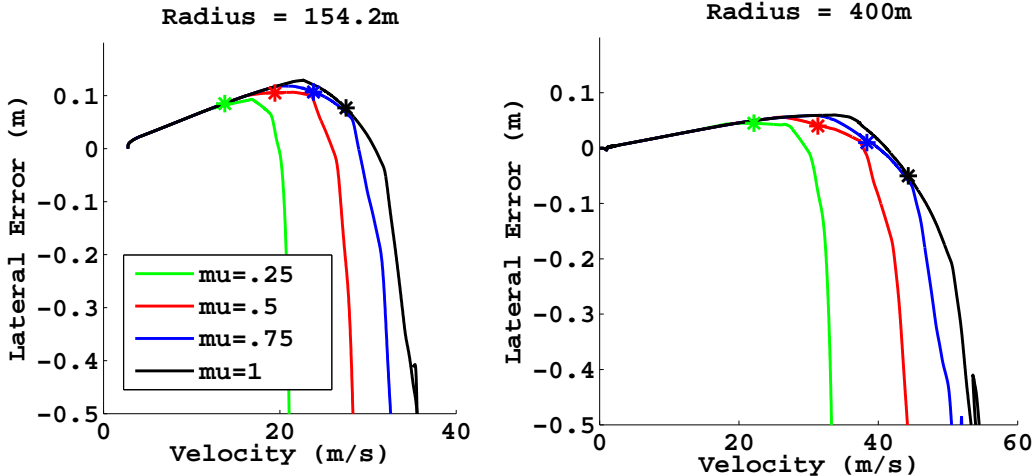


Figure 3.4: Predicting Slidout at Radius of 152.5 and 400 meters with the Dugoff Velocity Equation

Notice as the friction coefficient rises, the accuracy of the equations decrease. The reason the accuracy is decreasing could likely be from the effects of roll and weight transfer. During the simulation with a value of tire road friction of 1, nearly 80 percent of the weight was transferred to the outer tire. As the friction coefficient

rises, more weight is transferred to the outer tire before the vehicle reaches the limit of adhesion, causing all the vehicle's weight to be present on one tire instead of both. By assuming all the weight is on either the inner or outer tire, the steady-state tire slip angle can be recalculated resulting in a new Dugoff velocity equation.

$$V_{Dug} < \sqrt{\frac{\mu Rg}{4}} \tag{3.20}$$

This is a very simple change but will provide for safer results during periods of high roll angles. The experiments were repeated for the new Dugoff velocity and the results are shown in Figure 3.5 with the circles being the previous values using Equation (3.7).

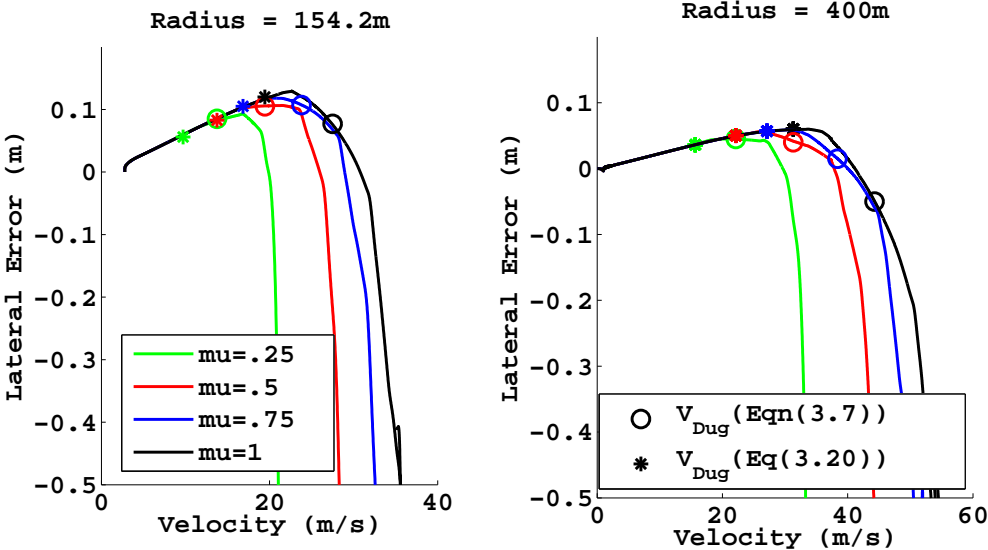


Figure 3.5: Predicting Slidout at Radius of 152.5 and 400 meters with the new Dugoff Velocity Equation

### 3.4.2 Rollover Equation

The rollover prediction formula was developed to help predict rollover during turning maneuvers. In this section, the formula is tested with different values of CG height on a 100 meter radius turn. The rollover prediction formula is a function of additional factors that have been evaluated by Lambert [21].

The first test run in this section is a simulation of a large SUV in Carsim slowly accelerating around a curve until rollover occurs. The values of this vehicle's parameters are shown in Appendix B. It is assumed rollover occurs when the all the weight of the vehicle is on the outer tires. Table 3.1 shows the simulated rollover speed versus the calculated rollover speed with each run having a different CG height. The results of this test show good correlation between the rollover prediction formula and the simulation's actual rollover.

Table 3.1 - Rollover Velocity on 100m Radius Turn

<i>CGHeight</i>	$V_{Rollover}$ from Sim. ( $\frac{m}{s}$ )	$V_{Rollover}$ from Eq. ( $\frac{m}{s}$ )	% Diff.
1.2	23.06	23.16	0.4 %
1.0	25.72	25.37	1.4 %
0.8	29.08	28.36	2.5 %
0.6	32.92	32.75	0.5 %

### 3.4.3 Stopping Distance

This section performs braking simulations in Carsim to test the effectiveness of the minimum stopping distance equation. The simulations consisted of multiple runs on roads with different tire-road friction ( $\mu$ ) values. All runs will use Carsim's

ABS system to assure quicker braking response and to also simulate how braking would occur in a real vehicle. Table 3.2 below shows simulated and calculated stopping distances (SD) for roads with different values of  $\mu$ .

Table 3.2 - Stopping Distance at  $V_o=30\frac{m}{s}$

$\mu$	SD from Sim. (m)	SD from Eq. (m)	% Diff.
0.25	189.3	183.5	3.06 %
0.5	94.3	91.7	2.76 %
0.75	60.9	61.2	0.49 %
1.0	45.4	45.9	1.10 %

Next, a set of simulations on a -15 degree incline were conducted. The simulations for this test consist of multiple runs on an incline with different  $\mu$  values. Table 3.3 shows the predicted and actual value of stopping distances for these simulations. The simulation with a coefficient of friction of 0.25 is listed as unknown. This is because the value of  $\sin(\theta)$  is greater than the value of  $\mu$  causing the vehicle to slide down the hill without slowing down. The simulation shows similar results with the vehicle never actually coming to a stop. Therefore, the stopping distance equation can be used to predict if the road slope is too steep for the vehicle to stop on. These simulations prove the effectiveness of this simple equation. Therefore, in platoons of autonomous vehicles these equations would be effective in deciding a safe following distance from the lead vehicle with a known value of  $\mu$ . In order to fully utilize the SD equations, The next chapter will focus on estimation of  $\mu$ .

Table 3.3 - Stopping Distance at  $V_o=30\frac{m}{s}$   $\theta=-15$  deg

$\mu$	SD from Sim. (m)	SD from Eq. (m)	% Diff.
0.25	unknown	unknown	unknown %
0.5	197.3	190.2	3.60 %
0.75	91.9	93.4	1.63 %
1.0	60.1	61.9	2.99 %

### 3.5 Conclusions

This chapter developed predicted velocities that proved to be effective at predicting rollover and sliding out even though many simplification were made to obtain the equations. An equation was also derived to calculate a speed that minimizes the sideslip angle at the vehicle's center of gravity. In order to calculate the predictive velocities, many important parameters must be known, such as the friction coefficient and the vehicle's center of gravity position. Stopping distance equations were derived and proved very effective at predicting the stopping distance of the vehicle assuming certain parameters are known, such as  $\mu$  and  $\theta$ . The predictive velocities were then validated with a series of simulations performed in Carsim. The results of those test showed very good correlation between the true speed of rollover and sliding out and the predicted values calculated by the predictive velocity equations derived in this chapter. In the next chapter, algorithms will be developed to obtain parameters needed for these equations.

## CHAPTER 4

### ESTIMATION ALGORITHM DEVELOPMENT

#### 4.1 Introduction

This chapter develops parameter estimation algorithms based off of the vehicle models shown in Chapter 2. The most important and difficult parameter to estimate may be tire-road friction, as it is used for the dugoff velocity and the stopping distance equations. To estimate this parameter, a non-linear tire model must be used that describes the tire's saturation. This chapter uses the Fiala and Dugoff tire model with a non-linear estimator to obtain an estimate of peak tire force. Other parameters that need to be estimated include the CG height and weight split. The weight split is estimated using the bicycle model in a non-linear estimator. To estimate CG height, a recursive least squares estimator is used. Estimates of these important parameters are necessary to update the predictive velocities and stopping distance equations developed in Chapter 3. Validation of the tire parameter and weight split estimation algorithms is conducted in MATLAB with data from the G35 sedan, discussed in Chapter 2. Simulations with Carsim's large SUV are used to validate the CG height estimator since a vehicle with a taller CG is desired.

## 4.2 Tire Parameter Estimates

Many researchers have developed methods to estimate tire parameters. While some researcher have used lateral vehicle models to achieve an estimate of cornering stiffness [32, 30], others have used lateral vehicle models along with non-linear tire models to estimate cornering stiffness and tire road friction simultaneously [6, 16]. Another method developed by previous researchers includes measurements of the steering wheel torque to achieve estimates of these two important parameters [17, 20, 23]. Some researchers have used longitudinal vehicle models to estimate the tire-road friction [4, 5]. In this section, a method will be developed to estimate lateral and longitudinal tire parameters using non-linear tire models, previously published in [8].

To estimate lateral and longitudinal tire stiffness as well as the peak tire force, some type of estimator must be chosen. Since non-linear tire models are used in this estimation, an extended Kalman filter (EKF) was selected. A basic Kalman filter is a recursive algorithm that optimizes the estimate by statistically weighting the accuracy of each measurement. The extended Kalman filter, shown in Equations (4.1-4.7), is similar to the basic Kalman filter except the state transition and observation models need to only be differentiable functions of the state, instead of linear functions.

Time Update

$$\hat{x}_{k|k-1} = f(\hat{x}_{k-1|k-1}, u_k) \quad (4.1)$$

$$P_{k|k-1} = F_k P_{k-1|k-1} F_k^T + Q_k \quad (4.2)$$

Measurement Update

$$\tilde{y}_k = z_k - h(\hat{x}_{k|k-1}) \quad (4.3)$$

$$S_k = H_k P_{k|k-1} H_k^T + R_k \quad (4.4)$$

$$K_k = P_{k|k-1} H_k^T S_k^{-1} \quad (4.5)$$

$$\hat{x}_{k|k} = \hat{x}_{k|k-1} + K_k \tilde{y}_k \quad (4.6)$$

$$P_k = (I - K_k H_k) P_{k|k-1} \quad (4.7)$$

Because the system used in this section is non-linear, the  $H$  and  $F$  matrix will simply be the Jacobian of the output( $h$ ) and state transition model( $f$ ) respectively, as shown below.

$$H_k = \left. \frac{\partial h}{\partial x} \right|_{\hat{x}_{k|k-1}} \quad (4.8)$$

$$F_k = \left. \frac{\partial f}{\partial x} \right|_{\hat{x}_{k|k-1}, u_k} \quad (4.9)$$



Using the EKF shown above, it is possible to estimate the three states, lateral, longitudinal tire stiffness, and peak tire force, discussed earlier by using the Fiala or Dugoff tire model. The EKF uses a non-linear tire model as the output matrix meaning the tire forces will need to be used as a measurement to compare against the model. Therefore, the measurement matrix ( $z$ ) will consist of the lateral and longitudinal tire forces per axle. To get these measurements, a simple measurement transition matrix can be developed from the FBD in Figure 4.1.

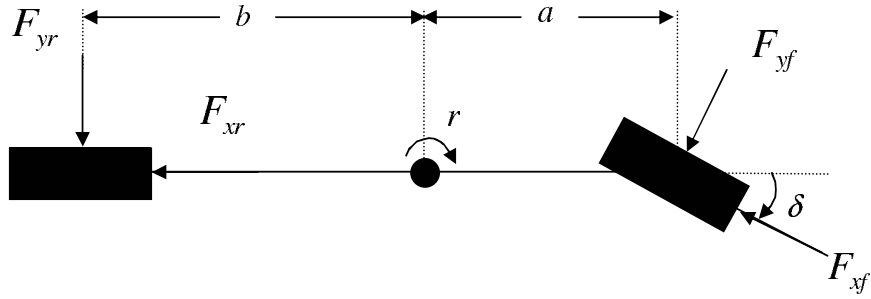


Figure 4.1: Tire Force Estimates

This figure is similar to the bicycle model earlier, except it also includes the longitudinal forces at the tires. All other assumptions used to develop the bicycle model in Chapter 2 are applicable for the force measurements derivation, shown in Equation (4.10) and (4.11).

$$\begin{bmatrix} ma_x \\ ma_y \\ I_z \dot{r} \\ 0 \end{bmatrix} = \begin{bmatrix} 1 & \cos(\delta) & 0 & -\sin(\delta) \\ 0 & \sin(\delta) & 1 & \cos(\delta) \\ 0 & a\sin(\delta) & -b & a\cos(\delta) \\ 0 & 1 & 0 & 0 \end{bmatrix} \begin{bmatrix} F_{xr} \\ F_{xf} \\ F_{yr} \\ F_{yf} \end{bmatrix} \quad \text{during acceleration (4.10)}$$

$$\begin{bmatrix} ma_x \\ ma_y \\ I_z \dot{r} \\ 0 \end{bmatrix} = \begin{bmatrix} 1 & \cos(\delta) & 0 & -\sin(\delta) \\ 0 & \sin(\delta) & 1 & \cos(\delta) \\ 0 & a\sin(\delta) & -b & a\cos(\delta) \\ -1 & 1 & 0 & 0 \end{bmatrix} \begin{bmatrix} F_{xr} \\ F_{xf} \\ F_{yr} \\ F_{yf} \end{bmatrix} \quad \text{during braking} \quad (4.11)$$

Inspection of the above equations show, the front longitudinal force is assumed to be zero during acceleration since the vehicle is rear wheel drive. Another assumption made is the front and rear longitudinal forces are equal during braking, although this may not always be true if the vehicle has a non 50-50 brake distribution. With an equation to calculate the tire forces, the performance of the EKF with the Dugoff or Fiala tire model can be further analyzed. The pros and cons of each tire model in conjunction with the EKF will also be explained in the following sections.

#### 4.2.1 Tire Stiffness and Peak Tire Force Estimation with Dugoff's Tire Model

To develop an extended Kalman filter using the Dugoff Tire Model to estimate lateral and longitudinal tire stiffness and peak tire force, Equations (2.24-2.27) will be needed. As shown in the last section, the  $z$  matrix must be composed of the lateral and longitudinal tire forces calculated with the transformation matrix.

$$z = \begin{bmatrix} F_x \\ F_y \end{bmatrix} \quad (4.12)$$

The state matrix ( $x$ ) is composed of the states that are to be identified.

$$x = \begin{bmatrix} C_\sigma \\ C_\alpha \\ \mu F_z \end{bmatrix} \quad (4.13)$$

The measurement matrix in Equation (4.12) can be used for the front or rear axle depending on which tire's properties need to be estimated. Since the state matrix is not changing as a function of time, the extended Kalman filter can be simplified similarly to the one used by Daily [6]. Because the system is non-linear with the states, the state transition matrix is simply the Jacobian of the tire force equations with respect to the states, shown by Equation (4.14).

$$H = \begin{bmatrix} \frac{\partial F_x}{\partial C_\sigma} & \frac{\partial F_x}{\partial C_\alpha} & \frac{\partial F_x}{\partial(\mu F_z)} \\ \frac{\partial F_y}{\partial C_\sigma} & \frac{\partial F_y}{\partial C_\alpha} & \frac{\partial F_y}{\partial(\mu F_z)} \end{bmatrix} \quad (4.14)$$

The Dugoff tire model has a transition when  $\lambda = 1$ , therefore two separate state matrices must be created. If  $\lambda < 1$  in the Dugoff tire model, the equations for the H matrix are listed below in Equations (4.15-4.20).

$$\frac{\partial F_x}{\partial C_\sigma} = \frac{\mu F_z \sigma C_\alpha^2 \tan^2(\alpha)}{((C_\sigma \sigma)^2 + (C_\alpha \tan(\alpha))^2)^{3/2}} - \frac{\sigma(1+\sigma)(\mu F_z)^2(-(C_\sigma \sigma)^2 + (C_\alpha \tan(\alpha))^2)}{4((C_\sigma \sigma)^2 + (C_\alpha \tan(\alpha))^2)^2} \quad (4.15)$$

$$\frac{\partial F_x}{\partial C_\alpha} = -\frac{\mu F_z \sigma C_\sigma C_\alpha \tan^2(\alpha)}{((C_\sigma \sigma)^2 + (C_\alpha \tan(\alpha))^2)^{3/2}} + \frac{C_\sigma \sigma(1+\sigma)(\mu F_z)^2 C_\alpha \tan^2(\alpha)}{2((C_\sigma \sigma)^2 + (C_\alpha \tan(\alpha))^2)^2} \quad (4.16)$$

$$\frac{\partial F_x}{\partial(\mu F_z)} = \frac{C_\sigma \sigma}{((C_\sigma \sigma)^2 + (C_\alpha \tan(\alpha))^2)^{1/2}} - \frac{C_\sigma \sigma(1+\sigma)\mu F_z}{2((C_\sigma \sigma)^2 + (C_\alpha \tan(\alpha))^2)} \quad (4.17)$$

$$\frac{\partial F_y}{\partial C_\sigma} = -\frac{\mu F_z \sigma^2 C_\sigma C_\alpha \tan(\alpha)}{((C_\sigma \sigma)^2 + (C_\alpha \tan(\alpha))^2)^{3/2}} + \frac{C_\sigma \sigma^2(1+\sigma)(\mu F_z)^2 C_\alpha \tan(\alpha)}{2((C_\sigma \sigma)^2 + (C_\alpha \tan(\alpha))^2)^2} \quad (4.18)$$

$$\frac{\partial F_y}{\partial C_\alpha} = \frac{\mu F_z \sigma^2 C_\sigma \tan(\alpha)}{((C_\sigma \sigma)^2 + (C_\alpha \tan(\alpha))^2)^{3/2}} - \frac{\tan(\alpha)(1+\sigma)(\mu F_z)^2(-(C_\sigma \sigma)^2 + (C_\alpha \tan(\alpha))^2)}{4((C_\sigma \sigma)^2 + (C_\alpha \tan(\alpha))^2)^2} \quad (4.19)$$

$$\frac{\partial F_y}{\partial(\mu F_z)} = \frac{C_\alpha \tan(\alpha)}{((C_\sigma \sigma)^2 + (C_\alpha \tan(\alpha))^2)^{1/2}} - \frac{C_\alpha \tan(\alpha)(1+\sigma)\mu F_z}{2((C_\sigma \sigma)^2 + (C_\alpha \tan(\alpha))^2)} \quad (4.20)$$

When the Dugoff Model transitions at  $\lambda = 1$ , the H matrix must be modified.

The equations for the H matrix when  $\lambda \geq 1$  are listed in Equations (4.21-4.26).

$$\frac{\partial F_x}{\partial C_\sigma} = \frac{\sigma}{1+\sigma} \quad (4.21)$$

$$\frac{\partial F_x}{\partial C_\alpha} = 0 \quad (4.22)$$

$$\frac{\partial F_x}{\partial(\mu F_z)} = 0 \quad (4.23)$$

$$\frac{\partial F_y}{\partial C_\sigma} = 0 \quad (4.24)$$

$$\frac{\partial F_y}{\partial C_\alpha} = \frac{\tan(\alpha)}{1+\sigma} \quad (4.25)$$

$$\frac{\partial F_y}{\partial(\mu F_z)} = 0 \quad (4.26)$$

Although the H matrix is very complex when the tire is saturated ( $\lambda < 1$ ), all states are observable. In contrast when the tire is in the linear region ( $\lambda \geq 1$ ),

the peak tire force is unobservable and cannot be estimated. It can also be seen that the lateral tire stiffness does not depend on the measurement of longitudinal tire force and the longitudinal tire stiffness is independent of the lateral tire force measurement. Because the peak tire force is unobservable, the EKF estimate of this parameter remains constant when  $\lambda \geq 1$ . This actually makes sense because the Dugoff tire model does not depend on the peak tire force to calculate the tire forces until the tire becomes saturated. Ideally, the peak tire force would be estimated before the tire becomes saturated to help limit the vehicle from sliding, but this is not possible using the Dugoff tire model. This leads to one advantage of using the Fiala tire model, as will be shown in the next section.

#### 4.2.2 Estimation with Fiala's Tire Model

In addition to the Dugoff tire model, the Fiala model can also be set up for estimation of certain tire properties. The measurement matrix remains the same as the one shown in Equation (4.12). Since the Fiala tire model assumes lateral and longitudinal tire stiffnesses are equal, the state matrix will be composed of only two states, peak tire force and tire stiffness depending on the maneuver. This simplification is shown in Equation (4.27).

$$x = \begin{bmatrix} C_{\sigma/\alpha} \\ \mu F_z \end{bmatrix} \quad (4.27)$$

The H matrix must also be calculated by taking the partial of the Fiala tire model (given previously in Equations (2.20-2.23)) with respect to the states in the state matrix. Like the Dugoff model, the Fiala model also has a model transition requiring two different H matrices depending on the value of  $\sigma$ . Equations (4.28-4.31) describe the H matrix if the tire is not saturated ( $\sigma \leq \sigma_m$ ).

$$\frac{\partial F_x}{\partial C_{\sigma/\alpha}} = \frac{\sigma_x [9(\mu F_z)^2 - 6C_{\sigma/\alpha} \mu F_z \sigma_t - C_{\sigma/\alpha}^2 \sigma_t^2]}{9(\mu F_z)^2} \quad (4.28)$$

$$\frac{\partial F_x}{\partial(\mu F_z)} = \frac{\sigma_t \sigma_x C_{\sigma/\alpha}^2 [9\mu F_z - 2C_{\sigma/\alpha} \sigma_t]}{27(\mu F_z)^3} \quad (4.29)$$

$$\frac{\partial F_y}{\partial C_{\sigma/\alpha}} = \frac{\sigma_y [9(\mu F_z)^2 - 6C_{\sigma/\alpha} \mu F_z \sigma_t - C_{\sigma/\alpha}^2 \sigma_t^2]}{9(\mu F_z)^2} \quad (4.30)$$

$$\frac{\partial F_y}{\partial(\mu F_z)} = \frac{\sigma_t \sigma_y C_{\sigma/\alpha}^2 [9\mu F_z - 2C_{\sigma/\alpha} \sigma_t]}{27(\mu F_z)^3} \quad (4.31)$$

However, if the tire begins sliding ( $\sigma \geq \sigma_m$ ) the H matrix will be composed of the following equations.

$$\frac{\partial F_x}{\partial C_{\sigma/\alpha}} = 0 \quad (4.32)$$

$$\frac{\partial F_x}{\partial(\mu F_z)} = \frac{\sigma_x}{\sigma_t} \quad (4.33)$$

$$\frac{\partial F_y}{\partial C_{\sigma/\alpha}} = 0 \quad (4.34)$$

$$\frac{\partial F_y}{\partial(\mu F_z)} = \frac{\sigma_y}{\sigma_t} \quad (4.35)$$

Unlike estimation with the Dugoff model, peak tire force can be estimated before and after the tire begins to slide. This is advantageous because the estimator may be able to predict the peak tire force before the tire begins to slide. However, the tire stiffness is unobservable when the tire begins to slide.

To estimate the tire stiffness and peak tire force with both the Fiala and Dugoff tire models, the  $Q$  and  $R$  matrix must be identified. The  $Q$  matrix is the process noise covariance matrix and is primarily composed of the standard deviation of the process noises. In this section the  $Q$  matrix acts like a forgetting factor in a recursive least squares algorithm [6]. The  $R$  matrix is the measurement noise covariance matrix and is composed of values of the noise covariances of the measurements. In this research, the true value for the process and measurement noise covariance matrices can not be determined analytically. Therefore, the values in the matrices were hand chosen to provide a quick rate of convergence. The matrices for estimation with the Dugoff model can be seen in Equations (4.36) and (4.37).

$$Q = 1e^{-8} \begin{bmatrix} (80,000N)^2 & 0 & 0 \\ 0 & (80,000N/rad)^2 & 0 \\ 0 & 0 & (12,000N)^2 \end{bmatrix} \quad (4.36)$$

$$R = \begin{bmatrix} (5,000N)^2 & 0 \\ 0 & (5,000N/rad)^2 \end{bmatrix} \quad (4.37)$$

Since estimation with the Fiala model only has two states, the  $Q$  matrix is reduced to:

$$Q = 1e^{-8} \begin{bmatrix} (80,000N/rad)^2 & 0 \\ 0 & (12,000N)^2 \end{bmatrix} \quad (4.38)$$

During periods of small excitation, the estimator may perform badly producing incorrect estimates of the states. One way to account for this is by adjusting the H matrix. If the vehicle is driving straight and not producing any lateral or longitudinal excitation, the H matrix can be set to zero. This will effectively hold all the prior estimates constant. Also during periods of longitudinal excitation only the elements of the H matrix that effect lateral dynamics can be set to zero to avoid a bad estimate of lateral tire stiffness, but still provide an accurate estimate of longitudinal tire stiffness and peak tire force.

### 4.3 Weight Split Estimation

In order to calculate the zero-sideslip velocity, the distance from the rear axle to the vehicle's center of gravity must be known. One method that may provide an accurate estimate would be using the bicycle model, shown in Equation (2.9), in a non-linear estimator. Ryu [30] used this model with a total least squares algorithm to estimate cornering stiffness and yaw moment of inertia simultaneously. The particular research also attempted to estimate cornering stiffness and weight split simultaneously using this method but was unsuccessful at converging to the correct values unless highly excited. A technique, previously published in [9] which uses



the bicycle model and an EKF, is used in this thesis to update the zero-sideslip velocity with the weight split estimate.

By augmenting the state space representation of the bicycle model, shown in Equation (2.9), in an estimator the weight split can be estimated. As discussed earlier, the bicycle model assumes no weight transfer and the tires are assumed to be in the linear region. The importance of this assumption will be discussed later. Because the system is non-linear with respect to the weight split and yaw moment of inertia, the extended Kalman filter is used. The EKF was earlier presented in Equations (4.1-4.7). In this algorithm, the states (parameter estimates) are assumed to be constant; therefore, the differential equations used to describe the system ( $f$ ) is simply equal to the process noise ( $w$ ), shown by Equation (4.39).

$$f = \begin{bmatrix} \dot{a} \\ \dot{I}_z \end{bmatrix} = w \quad (4.39)$$

By studying the above equation, the state matrix ( $x$ ) is composed of the distance from the front axle to the vehicle's center of gravity ( $a$ ) and the yaw moment of inertia ( $I_z$ ). The state matrix could also include the distance from the vehicle's CG to the rear axle ( $b$ ), but for simplification purposes this state is replaced by  $L - a$ . To describe the output of the system, Equation 4.40 is used.

$$z = \begin{bmatrix} a_y \\ \dot{r} \end{bmatrix} = H \begin{bmatrix} a \\ I_z \end{bmatrix} + v \quad (4.40)$$

The measurements included in this equation is the lateral acceleration ( $a_y$ ) and yaw angular acceleration ( $\dot{r}$ ). The measurements are equal to the observation matrix ( $H$ ) times the states plus the measurement noise. The H matrix comes from the linearization of the bicycle model with respect to the states being estimated. The observation matrix is shown below in Equation (4.41).

$$H = \begin{bmatrix} \frac{\partial a_y}{\partial a} & \frac{\partial a_y}{\partial I_z} \\ \frac{\partial \dot{r}}{\partial a} & \frac{\partial \dot{r}}{\partial I_z} \end{bmatrix} \quad (4.41)$$

where;

$$\frac{\partial a_y}{\partial a} = \frac{-(C_{\alpha f} + C_{\alpha r})r}{mV_x} \quad (4.42)$$

$$\frac{\partial a_y}{\partial I_z} = 0 \quad (4.43)$$

$$\frac{\partial \dot{r}}{\partial a} = \frac{-(C_{\alpha f} + C_{\alpha r})V_y}{I_z V_x} + \frac{(-2aC_{\alpha f} + 2(L - a)C_{\alpha r})r}{I_z V_x} + \frac{C_{\alpha f}\delta}{I_z} \quad (4.44)$$

$$\frac{\partial \dot{r}}{\partial I_z} = -\frac{(-aC_{\alpha f} + (L - a)C_{\alpha r})V_y}{I_z^2 V_x} - \frac{(-a^2 C_{\alpha f} - (L - a)^2 C_{\alpha r})r}{I_z^2 V_x} - \frac{aC_{\alpha f}\delta}{I_z^2} \quad (4.45)$$

Since the estimator is based off of the bicycle model, this model must accurately capture the actual dynamics in order for the estimated states to converge to the correct estimate. Therefore, knowledge of all the assumptions used in the bicycle model becomes critical. If the vehicle develops large roll angles or the vehicle generates large tire slip angles, the bicycle model cannot sufficiently capture the vehicle motion which will lead to errors in the estimated parameters.

#### 4.4 CG Height Estimation

One important parameter in rollover prevention is the height of the vehicle's center of gravity. With added weight on a vehicle, the CG height can shift up, increasing the chance of rollover. A recent researcher has investigated methods to estimate vehicle CG height using multiple models and switching and compared this method with recursive least squares [33, 34]. For this thesis, a recursive least squares algorithm is used to estimate the parameter, similar to [34], using the roll planer model as a measurement comparison. This will provide an estimate of CG height to update the predicted rollover velocity equation.

To begin the estimation algorithm development, recursive least squares (RLS) is briefly discussed. One author compared different recursive least squares techniques to estimate road grade and vehicle mass [35]. The methods used include recursive least squares, recursive least squares with forgetting factors, and recursive least squares with multiple forgetting. Since the parameters estimated in this section are assumed constant, the basic recursive least squares is used. If the parameters were changing, a forgetting factor could be used to forget old measurements. The basic least squares provides parameter estimates by minimizing the sum of the squares of the difference between the actually observed and the computed values [2]. To estimate the parameters on-line, the RLS Equations shown below are used.

$$\hat{\theta}_k = \hat{\theta}_{k-1} + L_k(y_k - \varphi_k^T \hat{\theta}_{k-1}) \quad (4.46)$$

$$L_k = P_k \varphi_k = P_{k-1} \varphi_k (1 + \varphi_k^T P_{k-1} \varphi_k) \quad (4.47)$$

$$P_k = (I - L_k \varphi_k^T) P_{k-1} \quad (4.48)$$

Equation (4.46) updates the estimate ( $\hat{\theta}_k$ ) by adding the previous estimate to an update gain ( $L_k$ ) times the error between the model output and the measurement ( $y_k$ ). This method is similar to the Kalman filter, but it does not utilize a time update thereby assuming the states remain constant. The variable,  $P_k$ , is known as the state estimation error covariance matrix and is usually initialized with a large value, due to uncertainty in the states. More information on the derivation and convergence of recursive least squares can be found in [35].

To estimate the CG height, the roll plane model, shown in Equations (2.30), is used. In order to utilize recursive least squares, the model equations must be linear. By assuming small angles the roll plane model can be rewritten, shown by Equation (4.49) [34].

$$a_y^{meas} = a_y + g\phi = \frac{1}{mh_{cg}} [J_{eff} \ddot{\phi} + C_\phi \dot{\phi} + K_\phi \phi] \quad (4.49)$$

Using a lateral acceleration measurement as the model input results in the state and regression vectors shown in Equations (4.50) and (4.51) respectively.

$$\varphi = \begin{bmatrix} \ddot{\phi} \\ \dot{\phi} \\ \phi \end{bmatrix} \quad (4.50)$$

$$\hat{\theta} = \begin{bmatrix} \frac{J_{eff}}{mh_{cg}} \\ \frac{C_{\phi}}{mh_{cg}} \\ \frac{K_{\phi}}{mh_{cg}} \end{bmatrix} \quad (4.51)$$

With a known value of roll mass moment of inertia ( $J_{eff}$ ), the parameters  $h_{cg}$ ,  $C_{\phi}$ , and  $K_{\phi}$  can easily be solved using simple algebra. The CG height will most likely change with added weight which will cause  $J_{eff}$  to also change. A better approach may be to estimate the value of  $J_{eff}$  and use a known value of  $K_{\phi}$  to solve for the CG height since  $K_{\phi}$  is less likely to change with added weight. Using this technique requires the roll dynamics to be excited and therefore must be conducted during a turning maneuver such as a lane change. Otherwise performing the estimation during straight driving could result in faulty estimates. The mass also needs to be known, as stated earlier. The mass can be estimated during acceleration or braking by [35], but it is assumed to be a known parameter in this thesis.

## 4.5 Experiments and Validation of Estimation Algorithms

To test the estimation algorithms, different experiments were performed in the Infiniti G35 Sedan and in Carsim. The tests performed help identify the effectiveness of the parameter estimation algorithms. If the algorithms are effective at providing accurate estimates, the algorithms can be used to update the vehicle controllers maximum speed around a curve or possibly even update control gains.

### 4.5.1 Experimental Setup

As discussed earlier, Carsim and an Infiniti G35 is used to validate the parameter estimation algorithms. Carsim is used to get realistic measurements to perform the estimation algorithms. The Infiniti G35 sedan is implemented with a dual antenna GPS unit, wheel speed sensor, a 6 DOF inertial measurement unit (IMU), and a optical encoder for steer angle measurements. Testing was performed at the National Center for Asphalt Technology (NCAT) test track in Opelika, AL. The IMU and wheel speed sensors provided measurements at 33 Hz, while the dual antenna GPS provided other necessary measurements at 5 Hz. Each subsection discusses in further detail the measurements that are important for each estimation algorithm.

### 4.5.2 Tire Parameter Estimation Experiments

To validate the tire estimation algorithms developed in Section 4.2, data was collected on the Infiniti G35 at the NCAT test track. To test the algorithm,

maneuvers consisted of pure lateral force generation, pure longitudinal acceleration, and a maneuver to achieve combined lateral and longitudinal force generation. The maneuvers are meant to fully saturate the tire to the point of sliding.

To collect the measurements for the measurement matrix, Equation (4.10) or (4.11) is used depending upon whether the vehicle is accelerating or braking. Therefore, both the lateral and longitudinal acceleration needs to be measured. These measurements are taken directly from the 6 DOF IMU. Another measurement needed for the calculation of tire forces is the yaw angular acceleration. This measurement is obtained by numerically differentiating the yaw rate gyro. Note that numerical differentiation increases the amount of noise already present in the yaw gyro.

For components of the H matrix, the lateral and longitudinal tire slips needs to be calculated. With measurements of wheel speed from the wheel speed sensors and velocity from the GPS, the longitudinal slip is simply calculated with Equations (2.18). When the vehicle is experiencing combined longitudinal and lateral force generation, the vehicle sideslip must be used to divide the velocity measurement from GPS into the lateral and longitudinal components. There have been many different studies to estimate the sideslip angle. The sideslip is defined as the difference between the vehicle heading ( $\psi$ ) and the vehicle course ( $\nu$ ) or direction of travel, as given below.

$$\beta = \nu - \psi \tag{4.52}$$

One method to obtain an estimate of sideslip is with a yaw gyro and GPS receiver. This method integrates the yaw gyro during turning to obtain an estimate of heading, while the yaw gyro bias is estimated during periods of straight driving [3]. With the estimate of heading, sideslip is easily calculated with Equation 4.52 if a course measurement is available. The course measurement can be easily obtained from GPS measurements. This is accomplished by comparing consecutive carrier measurements to provide a three dimensional velocity. Note that comparing consecutive measurements introduces a half sample delay that must be accounted for when processing the sideslip. Many errors arise from this method including: integration of a noisy gyro, scale factor errors, and incorrect bias estimates. Another author uses steering torque information to estimate the sideslip and is valuable during periods when GPS is unavailable [38]. The method used in this thesis uses a dual GPS antenna to get a measurement of heading. The dual GPS antenna provides this measurement by comparing carrier measurements at each antenna [31]. The heading measurement is then be subtracted from the course measurement, as discussed in the previous method.



With the sideslip measurement known at the GPS antenna (A), the velocity magnitude ( $V_{GPS}$ ) is broken up into lateral and longitudinal components.

$$V_x^{GPS} = V^{GPS} \cos(\beta^{GPS}) \quad (4.53)$$

$$V_y^{GPS} = V^{GPS} \sin(\beta^{GPS}) \quad (4.54)$$

Now the lateral and longitudinal velocities at the antenna are set up in vector form ( $\bar{V}_A$ ), This vector is easily transferred to the tires using Equation 4.55, where ( $\bar{V}_t$ ) is the velocity vector at the tire.

$$\bar{V}_t = \bar{V}_A + \bar{\omega} \times \bar{r}_{A/t} \quad (4.55)$$

In this equation,  $\bar{\omega}$  includes roll, pitch, and yaw angular velocities. The position vector,  $r_{A/t}$ , is defined from the antenna to the front or rear axle. With the above measurement of velocity at the tires, the longitudinal slip can then be calculated. Since the tire force calculation needs a value of wheel slip at the center of the axle, the average from the inner and outer tire is used. This assumption could be ineffective when the inner tire is experiencing high slip and the outer is hardly slipping. The lateral slip angle at the front and rear axle is then calculated from the lateral and longitudinal components of the tire velocity calculation in Equation (4.55).

$$\alpha_f = \tan^{-1} \left( \frac{V_y^f}{V_x^f} \right) - \delta \quad (4.56)$$

$$\alpha_r = \tan^{-1} \left( \frac{V_y^r}{V_x^r} \right) \quad (4.57)$$

In this equation,  $V_y^f$  is the lateral velocity at the center of the front axle and  $V_x^f$  is the longitudinal velocity at the front axle. The subscript,  $r$ , denotes the center of the rear axle.

### **Estimation during Lateral Dynamics Only Maneuver**

The first experiment conducted in the Infiniti G35 sedan includes lateral dynamics only. This test determines the effectiveness of using the Fiala and Dugoff tire models in an EKF by estimating the lateral tire stiffness and the peak tire force during periods of lateral excitation only. This maneuver consists of high speed cornering and a slalom at speeds ranging from 20 to 30 m/s. Figure 4.2 shows the experimental data input from the steering encoder and the response from yaw rate gyroscope.

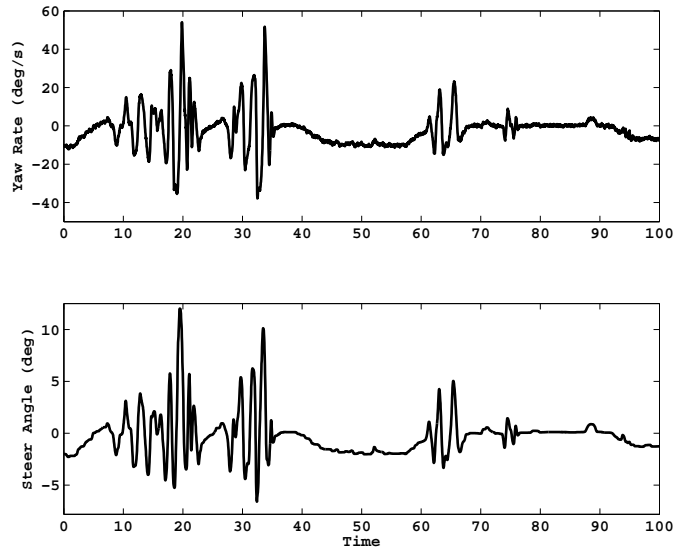


Figure 4.2: Lateral Experimental Data in the G35 Sedan used in the Tire Parameter Estimator [8]

Parameter estimation could be conducted using lateral force estimates only because the longitudinal dynamics are assumed to be negligible. However, this section is used to test the full algorithm and accounts for longitudinal measurements also. By simplifying the Dugoff or Fiala tire model to account for only lateral dynamics, the H matrix becomes much more simple.

With the experimental data at hand, MATLAB is used to conduct the estimation off-line. However, note that the estimation technique could be performed in real-time. Figure 4.3 shows the lateral tire stiffness and the peak tire force estimate. The longitudinal tire stiffness is not shown because the maneuver fails to sufficiently excite the longitudinal dynamics. The values shown are from the vehicle's rear axle. The peak tire force settles out in about 20 seconds. Notice for

estimation with the Dugoff tire model, the estimator does not update the peak tire force estimate until around 10 seconds. This is because the state is unobservable until the tire begins to saturate (i.e.  $\lambda < 1$ ). As explained earlier, the estimate remains constant until the tire becomes saturated. The lateral tire stiffness estimate settles out a little faster for estimation with the Fiala tire model, although both estimates converge closely to the same value. Appendix C shows additional tests using Carsim to validate the estimator used in this section.

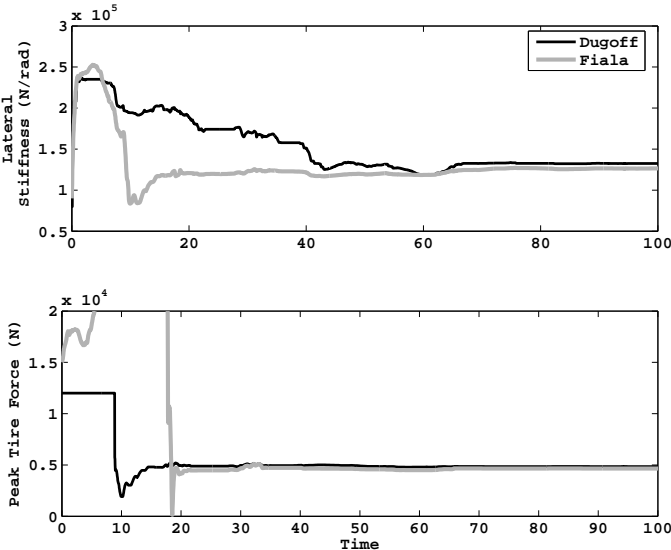


Figure 4.3: Lateral Tire Stiffness and Peak Tire Force Estimate from G35 Data during a Lateral Slalom [8]

**Estimation during Longitudinal Dynamics Only Maneuver**

The EKF will now tested for a maneuver that consists of heavy acceleration and braking in the test vehicle. The excessive accelerations can be seen in Figure

4.4 and are meant to reach the peak of the tire curve. Similar to the lateral only maneuver, this test is also conducted on an asphalt surface. On a lower friction surface, the maneuver would not need to be as severe to reach the limits of the tire.

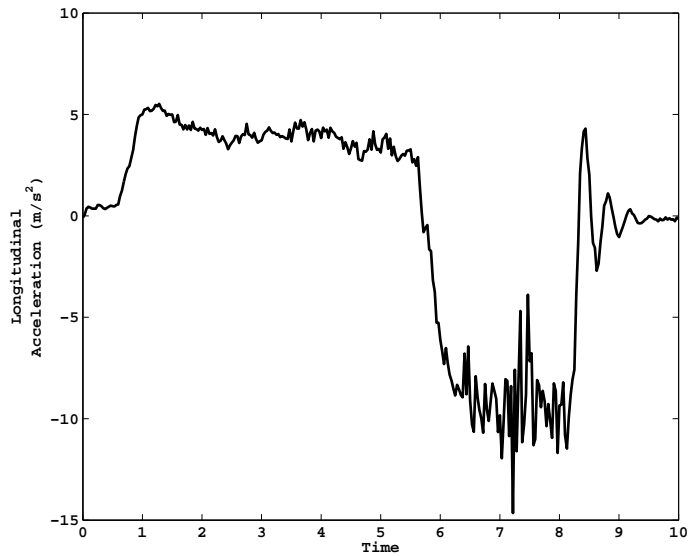


Figure 4.4: Longitudinal Acceleration in the G35 Sedan used in the Tire Estimator [8]

Lateral measurements are also included into the estimation, since the lateral dynamics are not excited the measurements contain mostly noise. Once again, the lateral dynamics could be left out by reducing the model to longitudinal forces only, but this section will test to determine if the noisy lateral measurements will effect the estimates.

As shown in Figure 4.5, the longitudinal tire stiffness settles out rather quickly and shows similar results using either the Fiala and Dugoff tire models in the tire

estimation algorithm. However, the estimate of longitudinal tire stiffness is not the same as the estimate for lateral tire stiffness. Recall that the Fiala tire model assumes the lateral and longitudinal stiffnesses are equal, therefore this will lead to errors in a combined maneuver. The peak tire force settles out slightly higher than the value estimated during lateral experiments in the previous section. Although the peak tire force for the longitudinal and lateral directions are assumed to be equal in this thesis, they could in fact be slightly different. Appendix C shows additional tests using Carsim to validate the estimator used in this section.

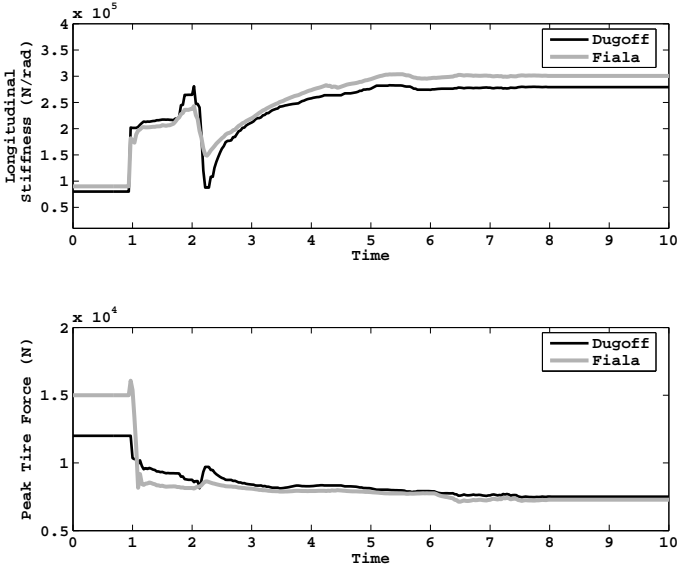


Figure 4.5: Longitudinal Stiffness and Peak Tire force Estimate from G35 Data during Acceleration and Braking[8]

## Estimation during Combined Lateral/Longitudinal Dynamics

The last maneuver conducted in the test vehicle was to test tire parameter estimation during a combined lateral/longitudinal maneuver. This test was done on a skid pad where the vehicle would brake and accelerate through turns. It highly excited both lateral and longitudinal dynamics. Figure 4.6 shows the output from the accelerometer and the yaw gyro during the combined lateral/longitudinal maneuver.

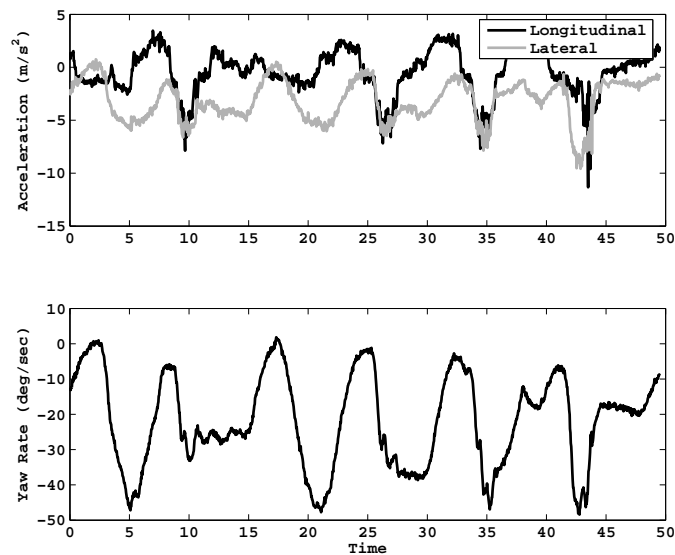


Figure 4.6: Accelerations and Yaw Rate Measurements for the Combined Lateral/Longitudinal Estimation [8]

As shown in the previous section, the lateral and longitudinal tire stiffness are not equal. Therefore, the tire estimation technique using the Dugoff tire model is used in this section. Figure 4.7 shows good correlation with previous plots with the values of lateral tire stiffness and peak tire force. However, the longitudinal tire

stiffness estimated shows a value much lower than that of the previous estimate.

This could be due to the inner and outer tires slipping at different rates.

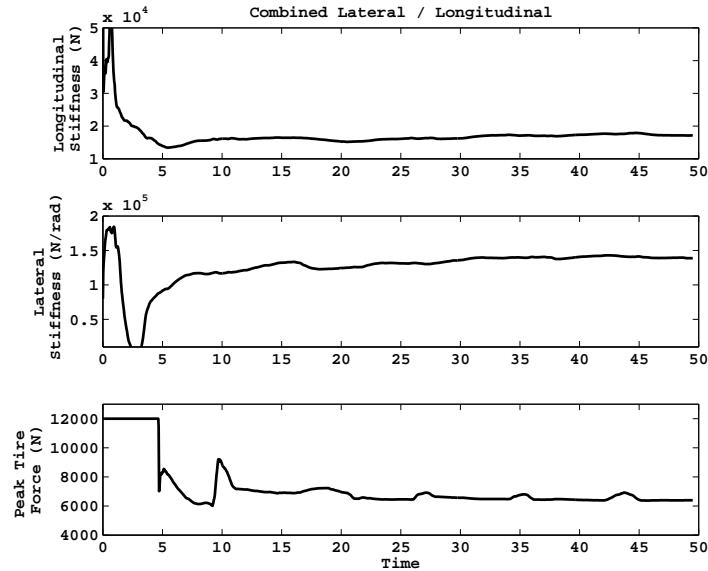


Figure 4.7: Tire Stiffness and Peak Tire Force Estimate during Lateral and Longitudinal Excitation of the G35 Sedan [8]

### 4.5.3 Weight Split Estimation Experiments

The weight split estimator is validated in this section by using data collected at NCAT test track in the Infiniti G35 sedan. Parameter values from this vehicle are shown in Appendix B. The measurements needed for this experiment are steer angle at the tire, lateral acceleration, yaw acceleration, and lateral and longitudinal velocity. These measurements are taken from this vehicle with a dual GPS receiver, IMU, and a steering encoder. Data was collected for validation of the weight split estimation algorithm during a 40 m/s turn in the test vehicle. The



lateral acceleration and yaw rate measurements for the maneuver used to test the algorithm is shown in Figure 4.8. These measurements are used as inputs to the estimator, presented in Section 4.3, to produce estimates of the weight split ( $a$  or  $b$ ) and yaw moment of inertia ( $I_z$ ).

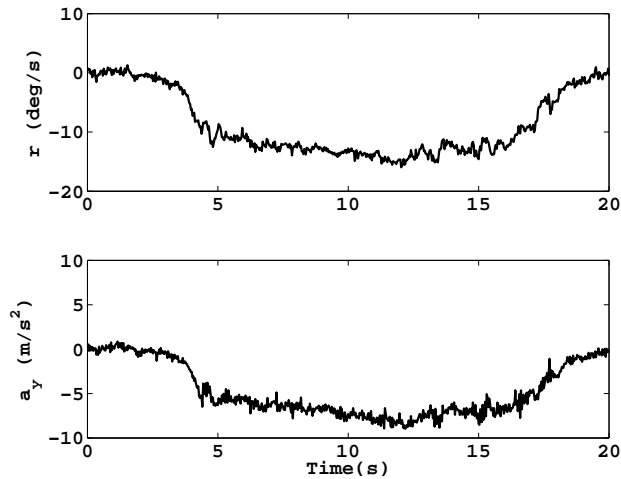


Figure 4.8: Cornering Data in the G35 Sedan at NCAT Test Track

Figure 4.9 shows the distance from the vehicle’s CG to the front axle converges closely to the values from the vehicle’s factory values of weight split. The yaw moment of inertia never completely settles out, possibly because the vehicle is performing a steady state turning maneuver with constant speeds and radius of turn providing little excitation. However, during maneuvers where the vehicle produces large slip angles, the weight split and yaw moment of inertia will be highly biased. This is due to the assumptions used to develop the bicycle model, which is used in the  $a$  and  $I_z$  estimation algorithm. For example, if the vehicle produces a large amount of roll the vehicle model will not match the data as well

as this example. Also if the tires saturate and begin to slide the assumption of a linear tire model breaks down. However, vehicles generally operate in the linear region of the tire with limited amounts of weight transfer, such that the algorithm should perform satisfactorily under normal driving conditions. More tests were conducted to test the algorithms performance using simulations in Carsim. These test are shown in Appendix C.

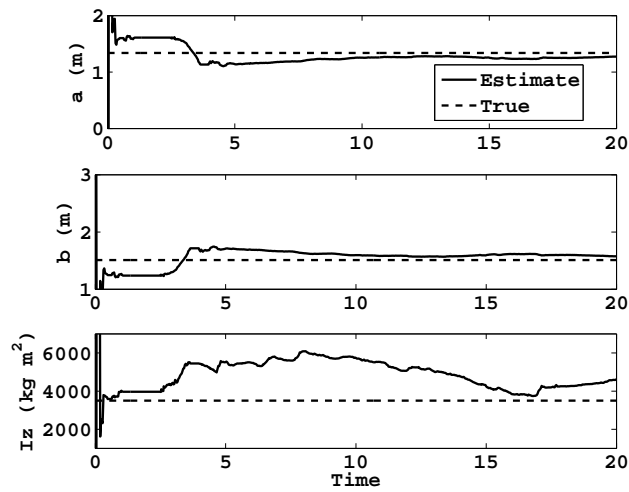


Figure 4.9: Weight Split,  $I_z$  Estimate During Cornering in the G35 Sedan

#### 4.5.4 CG Height Estimate Experiments

Some experiments estimating the CG height has already been published by [34]. The main difference in the CG height estimation algorithm used in this thesis is it assumes a known value for roll stiffness ( $K_\phi$ ) where the other work relies on the roll moment of inertia. One reason  $K_\phi$  was chosen is because it will not change with added weight like the roll moment of inertia will. To test this algorithm,

Carsim is used to provide a vehicle with a larger CG height. The simulations uses a large SUV that produces larger roll angles, as opposed to the G35 sedan. Values of the vehicle’s parameters used can be seen in Appendix B.

The Carsim output of lateral acceleration, roll, and roll velocity with the simulated sensor noise is shown in Figure 4.10. This data is used in the recursive least squares estimator to estimate the CG height, roll damping, and roll mass moment of inertia from the state matrix give previously in Equation 4.51. The vehicle performs a double lane change as can be seen in the figure.

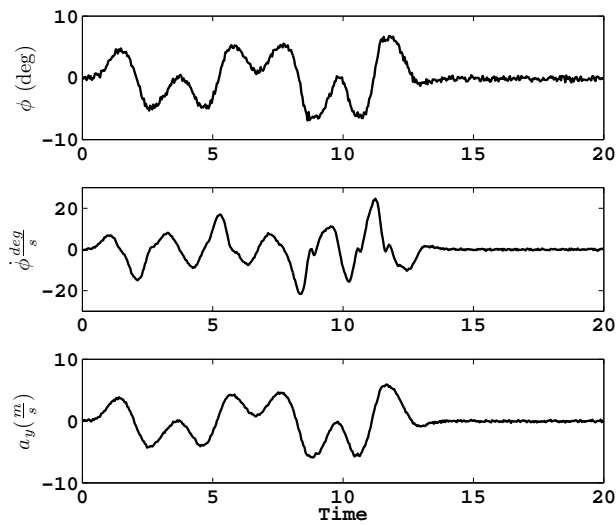


Figure 4.10: Double Lane Change with Added Noise in Carsim’s Large SUV

After the simulated data is generated in Carsim, Matlab is used to add artificial noise. Noise values can be found in Appendix B in the simulation parameter table. The Carsim data, with added noise, is then used as an input to the RLS algorithm given in Section 4.4. The plots in Figure 4.11 show the results of the

RLS algorithm including estimates of the CG height, roll damping, and the roll moment of inertia. The CG height estimate is slightly larger than the true value, however without injected noise in the simulation the estimate lies right on the true value. With increased noise levels, the estimate will rise slightly above the previous value. This is no surprise since it is well known that sensor noise can lead to biased estimates using RLS [39]. Although the estimate may be slightly off, the estimated value in this simulation always lies above the true value. Therefore, this acts as a safety factor when combined with the predictive rollover velocity, actually predict rollover at a slower speed. Although the roll mass moment of inertia does not converge to the correct value it is not used in the rollover prediction formula. The roll damping estimate converges closely to the true value but also is not used in the roll prediction velocity.

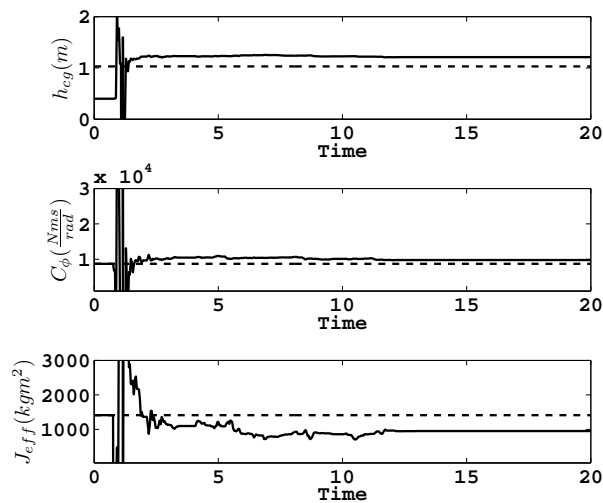


Figure 4.11: RLS Estimation of Large SUV’s CG Height, Roll Damping, and Roll Mass Moment of Inertia during a Double Lane Change in Carsim

## 4.6 Conclusion

This chapter described three different algorithms to assist in the estimation of important vehicle parameters. First, an extended Kalman filter was used to estimate the tire stiffness and peak tire force. The extended Kalman filter was chosen because the system to describe the saturation of the tire was non-linear. Two different non-linear tire models, the Fiala and Dugoff tire model, were implemented into the EKF and the pros and cons of estimating the tire parameters were discussed with each model. Next, an algorithm to estimate the vehicle's CG position and yaw moment of inertia was developed. This algorithm implemented the bicycle model into an EKF to perform the parameter estimation. The parameters were assumed to be constant in the derivation of the weight split estimation algorithm. The last algorithm developed in this chapter estimated CG height, roll damping, and roll mass moment of inertia. The roll dynamics that described the system were linear, therefore recursive least squares was chosen. To validate the tire parameter estimator data was collected in a G35 sedan at the NCAT test track. The tire parameter estimation algorithm was validated during a lateral, longitudinal, and combined vehicle dynamic maneuver. The weight split estimator was also validated with data from the G35 sedan, while the CG height estimator was validated using simulated data from Carsim. The limitations of each algorithm were also discussed in this chapter.

## CHAPTER 5

### UPDATED PREDICTIVE VELOCITY EXPERIMENTS

#### 5.1 Introduction

In this chapter, the predictive velocities are updated with parameter estimates discussed in the previous chapter in real-time. The experiments conducted provide safe look-ahead velocities to prevent rollover, sliding out, and also a minimum sideslip velocity for more dynamic maneuvers such as dodging something in the road. If the vehicle is following a leader, the parameter estimates could also be used to update a safe following distance. These experiments will use Carsim and Simulink together to simulate a true vehicle. This chapter is meant to show the usefulness of the parameter estimates in real-time. The parameter estimates could also be used for many other things such as updating control gains or limiting yaw rates, but in this chapter it will be used to limit the vehicle's velocity.

#### 5.2 Critical Velocity with Parameter Updates

The experimental setup uses data from Carsim that is exported in real-time to Simulink. The input into the Carsim model is the vehicle's desired velocity. This value is calculated in different sections depending on the maneuver and vehicle. This chapter also uses Carsim's velocity and steering controllers, but the desired values are sent directly to the velocity controller based upon the estimated

parameters and the turning radius. The turning radius is assumed to be known from the vehicle's path planner.

### 5.2.1 Zero Sideslip Velocity

The Zero Sideslip Velocity was derived in Chapter 3 and attempts to keep the value of sideslip to a minimum. This section will update this velocity with the estimation of weight split. This velocity is used during maneuvers with abrupt changes such as a lane change or dodging an object. The same measurements are needed as described in Section 4.5.3 and are obtainable with real sensors, but in this chapter the measurements are taken from Carsim on-line.

The first test conducted was a series of lane changes simulating a vehicle dodging an object. Figure 5.1 shows the path the vehicle attempts to follow at the desired speed calculated from Equation (3.7). Shown by the plot, the radius of curvature varies highly throughout the maneuver. The rollover velocity and Dugoff velocity is a function of radius of curvature, therefore may not be reasonable in this maneuver, this creates a need for the zero sideslip velocity. As the vehicle begins the lane change, the weight split, initially set at 50/50, is updated to speed up or slow down the vehicle. By doing this, the vehicle's sideslip is kept to a minimum. The derivation of the zero sideslip velocity assumes steady-state conditions, but that is not the case for this maneuver, therefore the sideslip cannot be constrained to zero.

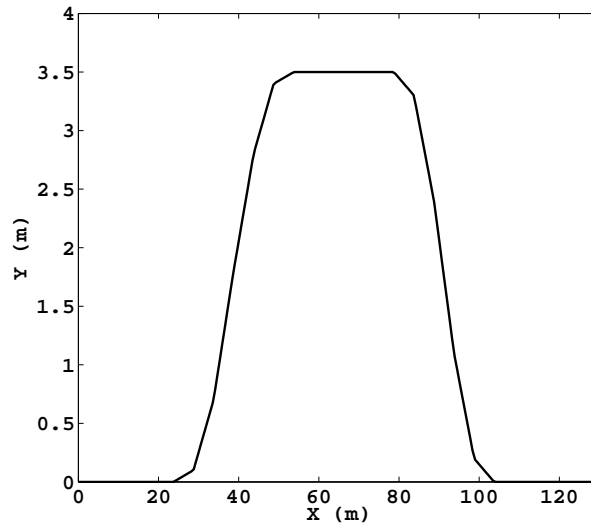


Figure 5.1: Desired Path for Vehicle Controlled at Zero Sideslip Velocity

Figure 5.2 shows the updated weight split for the vehicle. The estimates stay constant for about 1 second. This is because there is no input into the system, as the steering angle is initially zero until the maneuver begins. With this estimate of weight split, the desired velocity is updated.



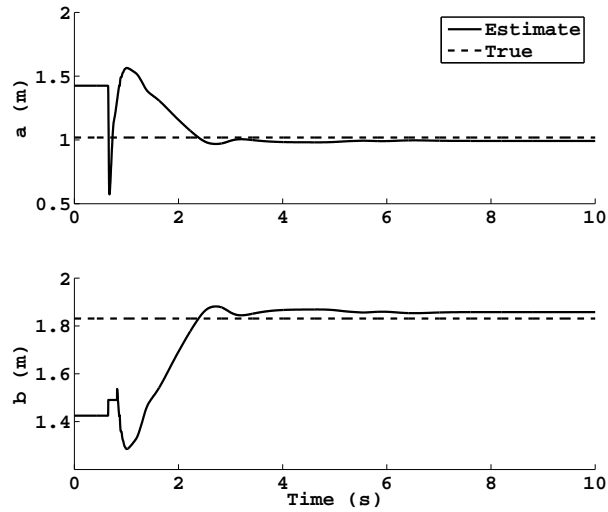


Figure 5.2: Weight Split Estimate in a Lane Change Maneuver at Zero Sideslip Velocity

Figure 5.3 shows the adaptation of the desired zero sideslip velocity, as it is updated with the estimate of  $b$ . The desired velocity is initially calculated to be 14.12 m/s with a 50/50 weight split. As soon as the vehicle enters the turn, the weight split estimator begins to estimate  $b$ . The updated value of  $b$  is used to update the desired velocity, plotted in 5.3. Carsim's velocity controller is used to drive the true speed to the desired speed. There is a little overshoot from the velocity controller but the vehicle quickly settles out the the desired speed.

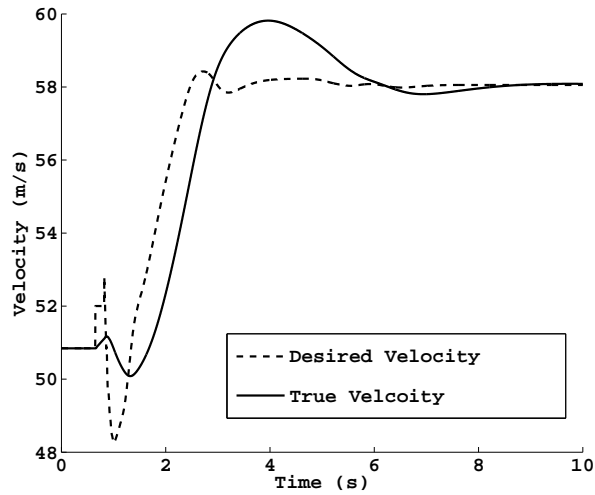


Figure 5.3: True and Desired Velocity Calculated from the Zero Sideslip Velocity in a Lane Change Maneuver in Carsim

Since the objective of this predictive velocity is to keep sideslip to a minimum, Figure 5.4 shows the values of the vehicle's sideslip controlled to the updated speed, shown in Figure 5.3, versus the sideslip from a vehicle without the weight split update. As discussed earlier, the vehicle is initially assumed to have a 50/50 weight split and travels at a constant speed of 14.12 m/s without the update of  $b$ . The above figure shows that the sideslip is in fact minimized by updating the zero sideslip velocity with an estimate of  $b$ . The sideslip in the plot is actually very similar until the velocity controller begins to settle out. This plot shows the effectiveness of this algorithm to minimize the sideslip during maneuvers such as a lane change.

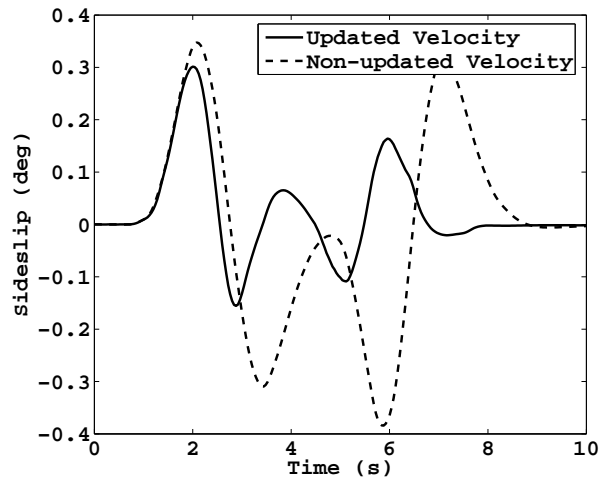


Figure 5.4: Sideslip with and without Desired Updated Velocity

### 5.2.2 Dugoff Velocity

The Dugoff velocity, derived in Equation (3.7), is used in this section to update the controlled velocity when the radius of curvature is not as variable as in the lane change. To do this, a method to estimate tire-road friction is used, developed in [29], to update the Dugoff velocity. The test is conducted in Carsim on a 400 m radius circle with a change in tire road friction. The friction coefficient drops from .85 to .5 over 100 meters. The updated and true coefficient of friction using the estimator is shown in Figure 5.5

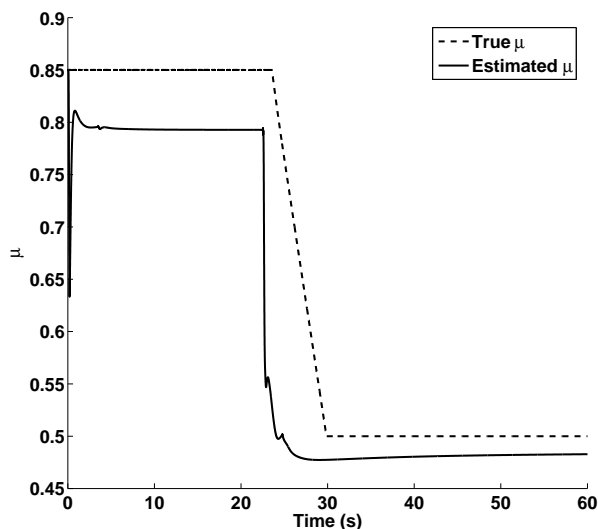


Figure 5.5: Coefficient of Friction Update during 400 Meter Radius Curve in Car-sim’s G35 Sedan

Notice that the estimate of the coefficient of friction is slightly lower than the true value. The reason for this may be that the system is not persistently excited. The maneuver the vehicle performs is at a steady state speed on a constant radius, therefore the inputs and outputs are very close to the same value until the coefficient of friction changes. Another problem with this method may be when the friction coefficient goes from a lower value to a higher value. This will be hard to detect because the vehicle will be traveling at a lower speed when the coefficient of friction changes, causing the tires to produce slip angles too small to estimate the friction coefficient.

As the friction coefficient is estimated, its value is used to calculate a desired speed from the Dugoff velocity equation. As stated in Section 3.2.2, the Dugoff

velocity equation is developed to ensure the tires remain inside the friction of circle during a steady state maneuver. Figure 5.6 provides the desired velocity to be controlled to and the vehicle's true velocity. Carsim's internal velocity controller is used to drive the true velocity to the desired value.

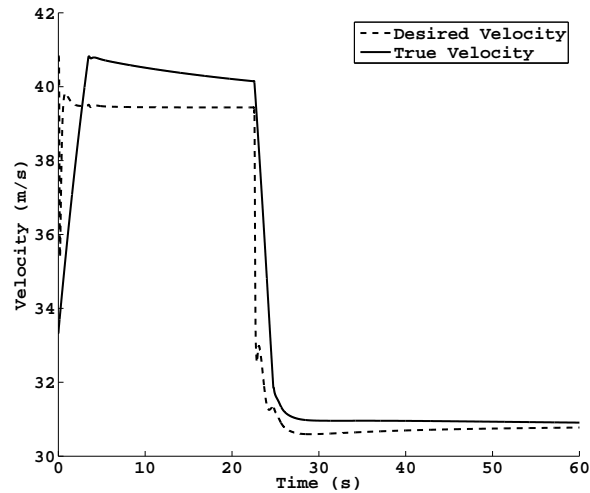


Figure 5.6: True and Desired Velocity Calculated from the Dugoff Velocity in a 400 m Radius turn in Carsim

Controlling the vehicle at the Dugoff velocity shows good results and provides sufficient excitation of the tire slip angles to provide an estimate of  $\mu$ . Figure 5.7 shows the values of the slip at the tires during this maneuver. Notice as the friction coefficient changes from a high to low value, the steady-state value of tire slip angle decreases. This is because with a lower value  $\mu$ , the roll dynamics are not effected as much as with the higher value. The effects of vehicle roll on the Dugoff velocity equation was discussed more in depth in Section 3.4.1. If the newer version of the Dugoff velocity equation is used, shown in Equation (3.20), the slip

angles produced at the tires are too small to accurately identify the value of the friction coefficient in this maneuver. Since it is generally not desired to produce large slip angles, the zero sideslip velocity could be used but the vehicle would be traveling at much slower speeds. For vehicle's with a large CG height, the rollover velocity must also be taken into account.

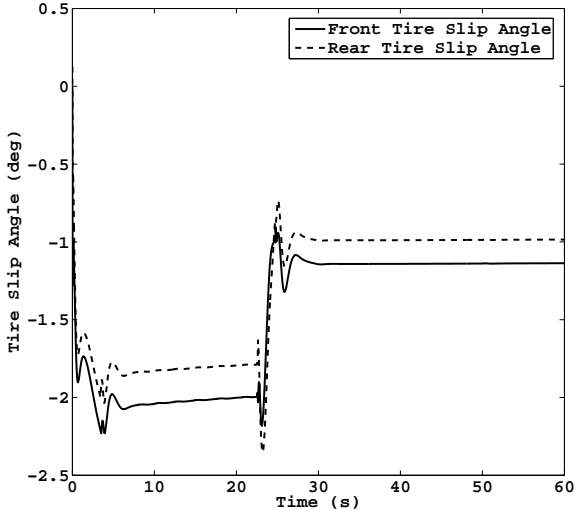


Figure 5.7: Tire Slip Angles in a 400 m Radius Turn with a Drop in Road Friction Coefficient while Controlling Speed at the Dugoff Velocity

With a varying radius of curvature, the velocity would oscillate depending on how much the radius is changing. During this, the smallest radius of curvature could be used to calculate a desired velocity. However, this would not ensure high enough slip angles for an accurate estimate of tire-road friction if the radius was changing from a high to low value.

### 5.2.3 Rollover Velocity

To help prevent rollover, it is beneficial to know minimum safe speeds for a vehicle to enter a turn. By updating the rollover velocity prediction formula with an estimate of CG height, this can be accomplished. Since the rollover formula predicts what velocity the vehicle will rollover, the limit velocity can be determined, assuming the radius of curvature is known. To test the method of updating the vehicle's velocity with a CG height estimate, a large SUV in Carsim will accelerate around a 200 meter radius turn. The vehicle will accelerate up to 90 % of the minimum rollover velocity calculated by Equation (3.12). If the vehicle is controlled to the minimum rollover velocity the vehicle will likely rollover with any controller overshoot. To reduce the number of parameters needed, the understeer gradient will be assumed to be equal to 0 (i.e. neutral steer vehicle) and the parameter to adjust for suspension effects,  $\kappa$ , will be set to .9. While the vehicle is accelerating up to the rollover velocity, the CG height will be estimated to update the minimum safe velocity. The algorithm used to estimate the CG height was shown in Section 4.4. Figure 5.8 shows the estimated CG height for this test.

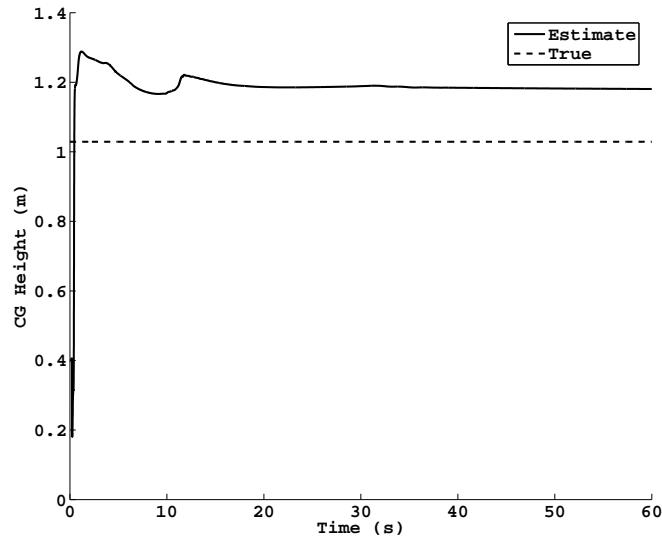


Figure 5.8: Estimated CG Height during a 400 m Radius Turn using data from Carsim’s Large SUV

In Figure 5.9, the desired and true vehicle velocities are shown. As shown by the plot, the velocity controller causes the true velocity to overshoot the desired velocity. If the minimum rollover velocity was used in this simulation, the controller overshoot would likely cause the vehicle to rollover. However, this simulation scaled down the rollover predictive velocity to 90 % of its true value to account for this. On roads with small variations in curvature, the roll dynamics would be excited more, causing a better estimate. In steady-state turns the roll dynamics are not highly excited.



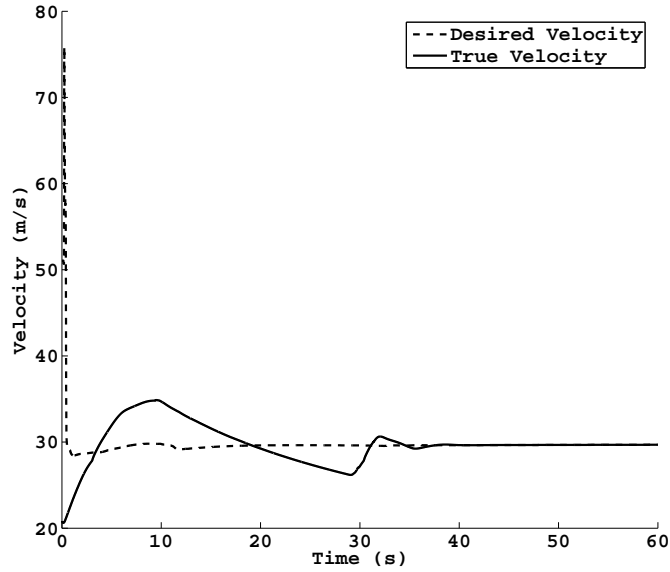


Figure 5.9: True and Desired Velocity Calculated from the Rollover Velocity in a 200 m Radius turn in Carsim

### 5.3 Conclusions

In this chapter, different experiments were conducted to show the usefulness of estimating important vehicle parameters in real-time. These test are mostly simple tests and could be conducted during different maneuvers or be used in different combinations, but are mostly used to show the importance of on-line parameter estimation. Tests performed included updating a desired velocity based on information from the path-planner, the vehicle, and the updated parameters. To be truly effective, a combination of the velocities would need to be included into the controller. For instance, in a larger vehicle the Dugoff and rollover predictive velocities would be calculated with the lower velocity being sent to the controller

as the desired velocity. Many other test could be performed to show the usefulness of these on-line estimates and provide an avenue for future work.

CHAPTER 6  
CONCLUSIONS

## 6.1 Overall Contributions

In this thesis, vehicle models were developed to describe the relationship between the inputs and outputs of the vehicle. These models were initially validated to show a match between the predicted outputs and true outputs. The models were then simplified to predict a velocity in which rollover and sliding occurs. A velocity equation was also developed to minimize the sideslip in a steady-state turn. By changing critical vehicle parameters in Carsim, the velocity equations were tested for accuracy and proved to be effective at predicting rollover and slideout, as well as minimizing sideslip. Additionally, experiments demonstrated that certain critical parameters highly effects the speeds at which a vehicle can maneuver a turn or lane change.

Because certain vehicle parameters have a large effect on vehicle handling, parameter estimation algorithms were developed. To estimate the tire-road friction coefficient and tire stiffness, a non-linear tire model was used in an extended Kalman filter. This method provided an estimate of the friction coefficient during periods of longitudinal and lateral tire force generation. Other parameters estimated included the CG position of the vehicle. Validation of the algorithms were also performed using different measurements which can be obtained from real sensors.

After the parameters were estimated, the critical velocity equations were updated to provide a safe look-ahead traveling speed. These parameters could also be used to update ESC systems. Simulations were ran to test the algorithms effectiveness during certain maneuvers in the vehicle. These simulations showed that by adjusting the vehicle speed to stay below the predictive velocity equations could be very beneficial to the safety of driven or autonomous vehicles.

## **6.2 Limitations**

Several limitations were identified in this thesis. For example, parameters can only be estimated when the vehicle's dynamics are being excited. Therefore, only during certain maneuvers are the predictive velocities able to be updated. However, during a maneuver that requires a velocity update, such as a turn or lane change, the vehicle is usually excited enough to get an estimate of various parameters. Also many of these estimates depend on measurements from a GPS receiver. These measurements can falter during periods of low satellite visibility.

## **6.3 Recommendations for Future Work**

During the research, it was realized that many other vehicle control systems could benefit from knowledge of unknown parameters. Certain vehicle control systems could set limits on vehicle states such as lateral velocity and yaw rate to reduce sliding out and rollover. With knowledge of changing vehicle parameters, these limits could be adjusted to take into account these states. By doing this,

many lives could be saved by reducing the number of accidents due to rollover and sliding off the road. The control systems also need accurate measurements of vehicle states such as sideslip. Since sideslip is expensive and difficult to measure, many researchers have developed model based systems to provide an estimate. By updating the model based systems with vehicle parameters using methods in this thesis, the model based state estimators could prove to be more effective in providing an accurate estimate.

The parameter estimation algorithms presented in this thesis could also be useful to Unmanned Ground Vehicles (UGVs). When traveling in platoons, it may be necessary to use the minimum stopping distance, calculated by Equation (3.19), to set the following distance or control the velocity. Some researchers have previously implemented throttle and braking controllers to maintain a constant following distance for vehicles in platoons [18]. By using the minimum stopping distance equation, the following distance in the platoon could be updated during maneuvers, such as a braking or turning, that could provide an estimate of tire road friction.

## BIBLIOGRAPHY

- [1] R. Anderson. "Using GPS for Model Based Estimation of Critical Vehicle States and Parameters". Master's thesis, Auburn University, 2004.
- [2] K. Astrom and B. Wittenmark. *Adaptive Control*. Addison Wesley, 1994.
- [3] D.M. Bevly, J.C. Gerdes, and C. Wilson. "The Use of GPS Based Velocity Measurements for Measurement of Sideslip and Wheel Slip". *Vehicle Systems Dynamics*, Vol. 38(2):pp127–147, 2002.
- [4] C.R. Carlson and 2002 Gerdes, J.C. "Identifying Tire Pressure Variation by Nonlinear Estimation of Longitudinal Stiffness and Effective Radius". In *Proc. AVEC 2002 6th INT. Symp. Advanced Vehicle Control*, 2002.
- [5] C.R. Carlson and J.C. Gerdes. "Consistent Nonlinear Estimation of Longitudinal Tire Stiffness and Effective Radius". *IEEE Transactions on Control Systems Technology*, Vol. 13, 2005.
- [6] R. Daily, W. Travis, and D.M. Bevly. "The Use of GPS Tire Parameter Estimates in a Model Based Estimator". *International Journal of Vehicle Autonomous Vehicles*, 2006.
- [7] H. Dugoff, P.S. Fancher, and L. Sengal. "Tyre Performance Charecteristics Affecting Vehicle Response to Steering and Braking Control Inputs". Technical report, Office of Vehicle Systems Research, US National Bureau of Standards, 1969.
- [8] Dustin Edwards. "A Method to Estimate Critical Tire Properties Using Non-Linear Tire Models". In *Proceedings of IMECE2007*, 2007.
- [9] Dustin Edwards. "Parameter Identification for Look-Ahead Maneuverability". In *AUVSIs Unmanned Systems North America 2007*. Auburn University, August 2007.
- [10] J. Farrlly and P. Wellstead. "Estimation of Vehicle Lateral Velocity". In *Proceedings from the 1996 IEEE Conference on Control Application*, 1996.
- [11] E Fiala. "Lareral Forces on Rolling Pnuematic Tires". *Zeitschrift V. D. I*, No. 29:96, 1954.

- [12] T. D. Gillespie. *Fundamentals of Vehicle Dynamics*. Society of Automotive Engineers, 1992.
- [13] R. Gunter and S. Sankar. "A Friction Circle Concept for Dugoff's Tyre Friction Model". *International Journal of Vehicle Design*, Vol. 1:pp373–377, 1980.
- [14] A. Hac. "Rollover Stability Index Including Effects of Suspension Design". *SAE Paper*, (2001-01-0965), 2002.
- [15] A Hac and M. Simpson. "Estimation of Vehicle Sideslip Angle and Yaw Rate". *SAE Paper Number 200-01-0696*, 2000.
- [16] J. Hahn, R. Rajamani, and L. Alexander. "GPS-Based Real-Time Identification of Tire-Road Friction Coefficient". Vol. 10, 2002.
- [17] Y.J. Hsu and J.C. Gerdes. "Stabilization of a Steer-By-Wire Vehicle at the Limits of Handling Using Feedback Linearization". In *Proceedings of IMECE2005*, 2005.
- [18] Hyun Mun Kim, Julie Dickerson, and Dart Kosko. "Fuzzy Throttle and Brake Control for Platoons of Smart Cars". *Fuzzy Sets and Systems*, Vol. 84:pp. 209–234, 1996.
- [19] T. M. Klein. "A Statistical Analysis of Vehicle Rollover Propensity and Vehicle Stability". *SAE Paper*, (920584), 1992.
- [20] S. Koo, H. Tan, and M Tomizuka. "Non-linear Tire Lateral Force Versus Slip Angle Curve Identification". In *Proceedings of the American Control Conference*, 2004.
- [21] Kenny Lambert. "A Study of the Properties That Influence Rollover and Their Effect on Electronic Stability Controllers". Master's thesis, Auburn University, 2007.
- [22] Bill Milliken and Doug Milliken. *Race Car Vehicle Dynamics*. Society of Automotive Engineers, 1995.
- [23] N.K. M'sirdi, A. Rabhi, N. Zbiri, and Y. Delanne. "Vehicle-Road Interaction Modeling for Estimation of Contact Forces". *Vehicle System Dynamics*, 43:pp 403–411, 2005.
- [24] G. Pacejka and R. S. Sharp. "Shear Force Development by Pnuematic Tires in Steady State Conditions. A Review of Modelling Aspects". *Vehicle System Dynamics*, Vol. 20:pp 121–176, 1991.

- [25] H. B. Pacejka, E. Bakker, and L. Lidner. "A New Tire Model with an Application in Vehicle Dynamics Studies". *SAE Paper*, (890087), 1989.
- [26] H. B. Pacejka, E. Bakker, and L. Nyborg. "Tyre Modelling for Use in Vehicle Dynamics Studies". *SAE Paper*, (870421), 1987.
- [27] Hans B. Pacejka and Egbert Bakker. "The Magic Formula Tyre Model". *Vehicle System Dynamics*, 21(1):1–18, 1992.
- [28] Desmond N. Penny. "Rollover of Sport Utility Vehicles". *The Physics Teacher*, 42:86–91, February 2004.
- [29] Rajesh Rajamani. *Vehicle Dynamics and Control*. Springer, 2006.
- [30] J. Ryu. "*State and Parameter Estimation for Vehicle Dynamics Using GPS*". PhD thesis, Stanford University, 2004.
- [31] J. Ryu, E.J. Rossetter, and J.C. Gerdes. "Vehicle Sideslip and Roll Parameter Estimation Using GPS". In *Proceedings of the AVAC 2002*, 2002.
- [32] C. Sierra, E. Tseng, A Jain, and H. Peng. "Cornering Stiffness Estimation Based on Vehicle Lateral Dynamics". *Vehicle System Dynamics*, 44:1:24–38, 2006.
- [33] Selim Solmaz, Mehmet Akar, and Robert Shorten. "Online Center of Gravity Estimation in Automotive Vehicles using Multiple Models and Switching". In *International Conference on Control, Automation, Robotics, and Vision*, 2006.
- [34] Selim Solmaz, Mehmet Akar, Robert Shorten, and Jens Kalluhl. "Realtime Multiple-Model Estimation of Center of Gravity Position in Automotive Vehicles". *Vehicle System Dynamics*, 2007.
- [35] A. Vahidi, A. Stefanopoulou, and H. Peng. "Recursive Least Squares with Forgetting for Online Estimation of Vehicle Mass and Road Grade: Theory and Experiments". *Vehicle System Dynamics*, Vol. 43:pp. 31–55, 2005.
- [36] Randall Whitehead, William Travis, David M. Bevly, and George Flowers. "A Study of the Effect of Various Vehicle Properties on Rollover Propensity". In *SAE International*, number 2004-01-2094. Auburn University, 2004.
- [37] Randall J. Whitehead. "A Study of the Properties That Influence Vehicle Rollover Propensity". Master's thesis, Auburn University, 2005.



- [38] P. Yih, J. Ryu, and J. C. Gerdes. "Vehicle State Estimation Using Steering Torque". In *Proceedings of the 2004 American Controls Conference*, volume Vol. 3, pages pp. 2116–2121, 2004.
- [39] Wei Xing Zheng. "Study of a Least-Squares-based Algorithm for Autoregressive Signals Subject to White Noise". *Mathematical Problems in Engineering*, Vol. 2003:pp. 93–101, 2003.

## APPENDICES

## APPENDIX A

### VEHICLE NOMENCLATURE

Chapter 2	
$a$	Length between CG and Front Contact Patch
$a_y$	Lateral Acceleration
$\alpha$	Tire Slip Angles
$b$	Length between CG and Rear Contact Patch
$\beta$	Sideslip Angle
$C$	Roll Damping
CG	Center of Gravity
$C_\alpha$	Lateral Tire Stiffness
$C_\sigma$	Longitudinal Tire Stiffness
$D_x$	Deceleration
$\delta$	Steer Angle
$F_y$	Tire Lateral Force (F, R)
$F_z$	Tire Vertical Force (F, R)
$g$	Acceleration due to Gravity
$h_{CG}$	CG Height
$I_z$	Yaw Moment of Inertia
$J_{eff}$	Roll Moment of Inertia
$K$	Roll Stiffness
$K_{us}$	Understeer Gradient
$L$	Length from Front Axle to Rear Axle
$m$	Vehicle Mass
$r$	Yaw Rate
$R$	Radius of Curvature
$T$	Track Width
$T_{spring}$	Torque from Springs
$T_{damper}$	Torque from Dampers

Chapter 2 cont.	
$V$	Vehicle Velocity
$V_x$	Vehicle Longitudinal Velocity
$V_y$	Vehicle Lateral Velocity
$\mu$	Tire Road Friction Coefficient
$\sigma$	Total Vehicle Slip
$\sigma_m$	Total Vehicle Slip in which sliding occurs
$\phi$	Vehicle Roll Angle
f = front      r = rear      L = Left      R = Right	

Chapter 3	
$D_x$	Deacceleration
SD	Stopping Distance
$V_{Dug}$	The Velocity the tire leaves the tire-friction circle
$V_{Rollover}$	The Velocity rollover occurs
$V_{\beta=0}$	The Velocity to minimize sideslip
$\theta$	Road Slope

Chapter 4	
$H_k$	Jacobian of Output Matix
$K_k$	Kalman Update Gain Matrix
$L_k$	Recursive Least Squares Update Gain
P	Covariance Matrix
R	Measurement Noise Covariance Matrix
Q	Process Noise Covariance Matrix
x	State Vector in EKF
z	Measurement Matrix in EKF
$\theta_k$	Recursive Least Squares State Matrix
$\nu$	Vehicle Course
$\psi$	Vehicle Heading

## APPENDIX B

### VEHICLE PROPERTIES

#### Properties of the G35 Sedan

Wheelbase:	$L$	2.8498 <i>m</i>
Vehicle Mass:	$m$	1528.2 <i>kg</i>
Dist. from CG to Front Contact Patch	$a$	1.3679 <i>m</i>
Dist. from CG to Rear Contact Patch	$b$	1.4819 <i>m</i>
Yaw Moment of Inertia	$I_z$	2400 <i>kg * m<sup>2</sup></i>
Front Tire Cornering Stiffness	$C_{\alpha f}$	91674 <i>N/rad</i>
Rear Tire Cornering Stiffness	$C_{\alpha r}$	152788 <i>N/rad</i>
Road Friction Coefficient	$\mu$	.85

#### Properties of Carsim's Large SUV

Vehicle Mass:	$m$	2450 <i>kg</i>
CG Height (Sprung Mass):	$h_{CG}$	1.1 <i>m</i>
Roll Mass Moment of Inertia	$J_{eff}$	1243 <i>kg * m<sup>2</sup></i>
Roll Stiffness	$K_{\phi}$	2527.9 $\frac{N-m}{deg}$
Roll Damping	$C_{\phi}$	152.05 $\frac{N-m-s}{deg}$
Track Width	$T$	1.62 <i>m</i>
Injected Noise Value on $a_y$	$\sigma_{a_y}^2$	(.1 <i>m/s<sup>2</sup></i> ) <sup>2</sup>
Injected Noise Value on $\phi$	$\sigma_{\phi}^2$	(.01 <i>rad</i> ) <sup>2</sup>
Injected Noise Value on $\dot{\phi}$	$\sigma_{\dot{\phi}}^2$	(.005 <i>rad/s</i> ) <sup>2</sup>

### Properties of Carsim's G35 Sedan

Wheelbase:	$L$	2.85 $m$
Vehicle Mass:	$m$	940 $kg$
Dist. from CG to Front Contact Patch	$a$	1.019 $m$
Dist. from CG to Rear Contact Patch	$b$	1.831 $m$
Yaw Moment of Inertia	$I_z$	1530 $kg * m^2$
Front Tire Cornering Stiffness	$C_{\alpha f}$	78311 $N/rad$
Rear Tire Cornering Stiffness	$C_{\alpha r}$	47033 $N/rad$
Injected Noise Value on $a_y$	$\sigma_{a_y}^2$	$(.1 \text{ m/s}^2)^2$
Injected Noise Value on $r$	$\sigma_r^2$	$(.02 \text{ rad/s})^2$
Injected Noise Value on $\beta$	$\sigma_{\beta}^2$	$(.02 \text{ rad})^2$
Injected Noise Value on $V$	$\sigma_V^2$	$(.01 \text{ m/s})^2$

## APPENDIX C

### TIRE PARAMETER AND WEIGHT SPLIT ESTIMATES USING DATA FROM CARSIM

#### **C.1 Tire Parameter Estimator Validation with Carsim’s G35 Sedan**

The estimator developed in Section 4.2 is shown in this section to test its effectiveness with data from Carsim. In Carsim, it is possible to know the true values of the vehicle parameters unlike the parameters in the Infiniti G35 Sedan used earlier to test with. Both the Fiala and Dugoff tire models are once again used to estimate the tire parameters

##### **C.1.1 Tire Parameter Estimator Testing during Lateral Maneuver**

A simulation is ran in Carsim to test the tire parameter estimation algorithm during a slalom in a G35 sedan. The lateral acceleration and yaw rate from the simulation is shown in Figure C.1. The vehicle reaches excessive lateral acceleration in this maneuver, enough so to saturate the tire enough for an estimate of peak tire force.

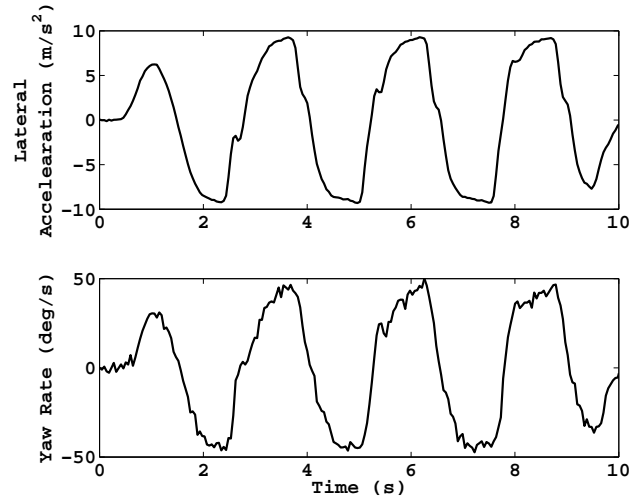


Figure C.1: Slalom in Carsim’s G35 Sedan

The data collected from Carsim is ran through the tire parameter estimator discussed in Section 4.2 to test the effectiveness of estimating lateral tire stiffness and peak tire force. Artificial zero mean random noise is added into the measurements to try to produce as real of a situation as possible. Values of the artificial zero mean random noise used in this simulation is shown in Appendix B along with the vehicle’s parameters. The true value of lateral tire stiffness is obtained by interpolating the experimental tire curve used by Carsim. Note that the value produced depends on what part of Carsim’s tire curve is assumed to be in the linear region and may fluctuate depending on different models. Since the Fiala and Dugoff tire models assume saturation of the tire occurs at different points on the tire curve their values may be different for tire stiffness. The values from from the estimator are shown in Figure C.2.



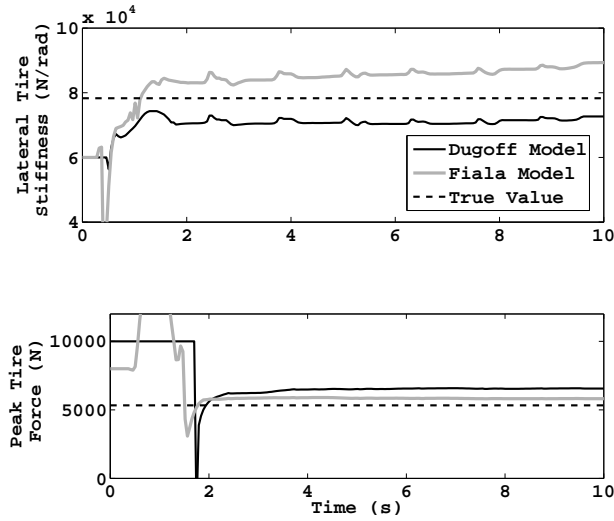


Figure C.2: Estimation of Tire Parameters during Slalom Maneuver

Once again the estimator with the Dugoff tire model does not begin estimating peak tire force until the tire begins to saturate. When the estimate begins to converge it lies slightly above the true value of peak tire force. It may also be noted that the Fiala model does not accurately converge until the tire is saturated, similarly to the test performed in Section 4.5.2.

### C.1.2 Tire Parameter Estimator Testing during Longitudinal Maneuver

The EKF will now tested for a maneuver that consists of heavy acceleration and braking in Carsim's G35 sedan. The excessive accelerations can be seen in Figure C.3 and are meant to reach the peak of the tire curve. Similar to the lateral only maneuver, this test is also conducted on an asphalt surface. On a

lower friction surface, the maneuver would not need to be as severe to reach the limits of the tire.

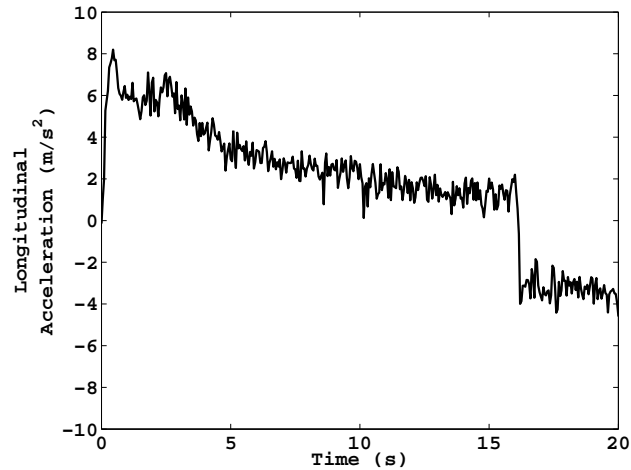


Figure C.3: Acceleration / Braking in Carsim's G35 Sedan

As shown in Figure C.4, the longitudinal tire stiffness settles out rather quickly and shows similar results using either the Fiala and Dugoff tire models in the tire estimation algorithm. However, the estimate of longitudinal tire stiffness is not the same as the estimate for lateral tire stiffness. Recall that the Fiala tire model assumes the lateral and longitudinal stiffnesses are equal, therefore this will lead to errors in a combined maneuver. The peak tire force settles out slightly lower than the value estimated during lateral experiments in the previous section. Although the peak tire force for the longitudinal and lateral directions are assumed to be equal in this thesis, they could in fact be slightly different.

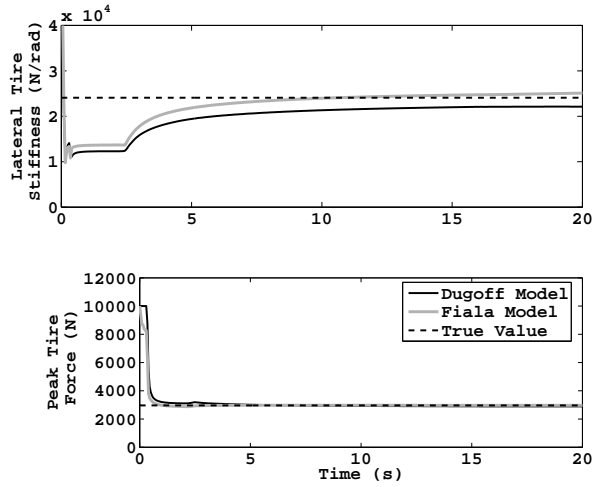


Figure C.4: Estimation of Tire Parameters during Acceleration / Braking Maneuver

## C.2 Weight Split Estimator Validation with Carsim’s G35 Sedan

The weight split estimator will be validated in this section by using data of a G35 sedan from Carsim. Parameter values from this vehicle are shown in Appendix B. Simulated experiments are conducted to show the effectiveness of the estimator to provide information on the weight split, and the shortcomings of this algorithm are also discussed. The measurements needed for this experiment are steer angle at the tire, lateral acceleration, yaw acceleration, and lateral and longitudinal velocity. These measurements can be taken from a real vehicle with a dual GPS receiver, IMU, and a steering encoder. However in this experiment, the data is taken directly from Carsim. The maneuver performed in the vehicle is a simple double lane change that would be performed during obstacle avoidance. The steering input, lateral acceleration, and yaw rate measurements for the double

lane change is shown in Figure C.5. Artificial zero mean random noise is added into the measurements to try to produce as real of a situation as possible. Values of the artificial zero mean random noise used in this simulation is shown in Appendix B along with the vehicle's parameters.

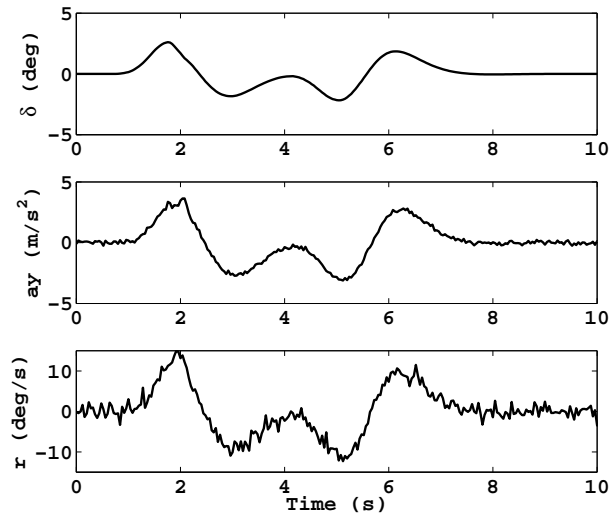


Figure C.5: Double Lane Change with Added Noise in Carsim

These measurements are used as inputs to the estimator, presented in Section 4.3, to produce estimates of the weight split ( $a$  or  $b$ ) and yaw moment of inertia ( $I_z$ ). Figure C.6 shows the distance from the vehicle's CG to the front axle converges to within .02 % of the actual CG location. Although the yaw moment of inertia never completely settles out, it does provide a good estimate of the parameter.

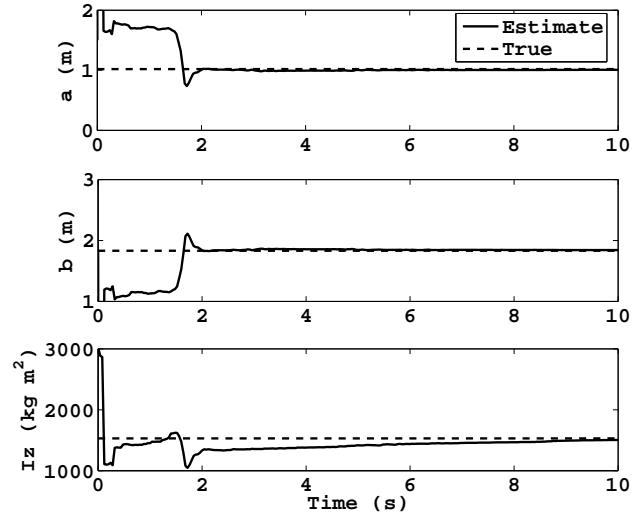


Figure C.6: Weight Split,  $I_z$  Estimate